3D-AFM Measurements for Semiconductor Structures and Devices

Ndubuisi G. Orji and Ronald G. Dixson

Engineering Physics Division
Physical Measurement Laboratory
National Institute of Standards and Technology
Gaithersburg, MD, 20899, USA

Abstract

This book chapter reviews different types of three-dimensional atomic force microscope (3D-AFM) measurements for semiconductor metrology. It covers different implementations of 3D-AFM, calibrations methods, measurement uncertainty considerations and applications. The goal is to outline key aspects of 3D-AFM for dimensional semiconductor measurements in a way that is accessible to both new and experienced users and gives readers a strong foundation for further study.

Preprint version

For published version see:

N. G. Orji & R. G. Dixson "3D-AFM Measurements for Semiconductor Structures and Devices" In *Metrology and Diagnostic Techniques for Nanoelectronics* (eds. Z. Ma, & D. G. Seiler) (Pan Stanford, 2017).

Table of Contents

1. INTRODUCTION

The pace of development and proliferation of atomic force microscope (AFM) technology is unprecedented in the history of microscopic imaging. Broad based adoption of AFM technology in different fields has led to a routine presence of conventional AFMs from college teaching laboratories to analytical service providers and to widespread use in research ranging from materials science to life sciences. The different types of AFM imaging modes and contrast mechanisms are now far too numerous and diverse for a typical user to be familiar with all of them. Applications of AFM now range from roughness metrology of ultra-smooth surfaces to the localized measurement of the mechanical properties of soft polymers. In addition to imaging modes based on topographic sensing, contrast modes sensitive to the electrical, magnetic, and chemical properties of surfaces are also available [1-4]. Conventional AFM is also described as one dimensional or 1D-AFM. This is because the tip to sample separation is usually only servoed along a single axis – the vertical or z-axis. Even when cantilever deflection is detected in two axes, such as in lateral or friction force microscopy, the only position feedback applied to the tip-sample separation is in the z-axis[5].

One limitation of conventional AFM is the inability to access and measure vertical features, such as the sidewalls of patterned semiconductor lines. Given the importance of controlling process variability in semiconductor manufacturing, there was a need for feature metrology with capabilities beyond those of 1D-AFM. This requirement drove the development of advanced AFM technologies, some of which are referred to as three dimensional or 3D-AFM.

Consequently, the primary application space of 3D-AFM technology is dimensional metrology of lithographically patterned nano-structures in semiconductor manufacturing, and, therefore, this is also the focus of this chapter. 3D-AFM technology is considerably more sophisticated and expensive than conventional AFM and so is less widely used. The goal of the chapter is to describe some of the key applications of 3D-AFM in semiconductor dimensional metrology and the steps needed to achieve accurate and consistent measurements.

1.1 A Note on Dimensionality of AFMs

The ability of the AFM tip to scan over a specified range and produce height information as a function of x and y position means that AFM data is generally referred to as three dimensional even though the image formation physics relies primarily on the tip-sample interaction in a single (vertical) axis. Hence, from the perspective of the data sets that can be acquired, all AFMs are capable of generating three-dimensional images. In particular contrast with the first 50 years of two-dimensional stylus profiling, it could thus be said that all AFMs are three dimensional.

But this excessively simplifies the situation, since there are more characteristics of an AFM in need of description than the apparent dimensions of an image. Conventional AFMs suffer from both significant functional constraints and imaging artifacts that render them less than truly three dimensional. A particularly important example which was mentioned above is the limitation of tip-sample position control to a single axis. Another example is that shape of most conventional AFM tips is tapered such that near-vertical sidewalls are geometrically occluded and cannot be imaged [6]. The AFM methods described in this chapter are techniques capable of providing near-vertical sidewall data by utilizing some combination of specially shaped tips, advanced data acquisition strategies, and multi-axis detection and control of the tip-sample interaction. However, even current generation tools do not have three axes equivalence in terms of force sensing, displacement accuracy, or tip position control. To state this more explicitly, *a true 3D-AFM with regards to force sensing and data acquisition in three axes does not exist at the time of this review*. One should think of the term “3D-AFM” as representing a certain type of AFM, rather than one where force sensing and extraction is available in three dimensions. Our use of the term is in line with this representation. Later in the chapter we address some of the requirements of a true 3D-AFM.

1.2 Implementations of 3D-AFM

To date, there have been at least five distinct implementations of advanced AFM technology that have been or could be described as 3DAFM. For purposes of this chapter, all of these methods will be regarded as implementations of 3D-AFM, although none is fully three dimensional in every possible sense. An early implementation of AFM that was capable of steep-sidewall metrology was by Nyssonnen et al. [7]. This system utilized three pointed tips with apexes aligned in the lateral axes in order to have geometrical access to near-vertical sidewalls. Another significant and distinguishing feature of this method was that it used resonant detection of cantilever vibration in both lateral and vertical axes. However, this approach was never commercialized. Also, in the early 1990s, other investigators worked on methods to mitigate the imaging and tip limitations of conventional AFM. For example, Griffith et al. developed a system for metrology of high aspect ratio structures [6, 8]. Some of the unique features of their approach were an electrostatic balance beam force sensor and the use of very sharp and near-cylindrical tips. Although their approach improved significantly over the performance of conventional AFM at the time, it did not utilize multi-axis vibration of the tip as some other 3D-AFM techniques do. Although this implementation was commercialized for a few years, it did not achieve widespread acceptance. The most commercially prevalent 3D-AFM implementation today was also developed in the early 1990s [9]. It is now most commonly referred to as critical dimension AFM (CD-AFM). The most salient features of this method are the use of flared tips, sub-resonant lateral dithering of the tip in addition to the near-resonant vertical oscillation of the cantilever, and a bidirectional servo and feedback system. This combination allows the imaging of vertical and reentrant sidewalls, which are crucial to quantifying 3D features. A schematic diagram of the CD-AFM mode is shown in Fig. 1.

To accurately detect surface topography along the sidewall, this method used an implementation of adaptive data spacing. Essentially, this means that data are acquired at points based on the sidewall topography rather than using a fixed spacing in the lateral axis - which is typical in conventional AFM. This innovation enabled the measurement of parameters such as sidewall angles[10], linewidth variability, and sidewall roughness[11], which are crucial to quantifying 3D features. To accommodate vertical and reentrant sidewalls, the CD-AFM data format must support multiple z-axis values at a given lateral position. Although key performance and usability improvements [12-14] have been made over the years, the basic principles of CD-AFM technology are still the same.

Subsequently, Morimoto, Watanabe, et al. developed an AFM method for imaging steep sidewalls [15, 16]. A central feature of their approach was a scanning algorithm that involved retracting and stepping the tip rather than maintaining continuous contact. The advantage of this method is that the steep-edge artifacts that result from tip bending and the z-axis feedback loop in conventional AFM are mitigated with the step-in approach. Their system was also able to use sharp tips – including carbon nanotube (CNT) tips to maximum advantage because it could leverage the attractive bending of the CNT toward the sidewall for purposes of imaging. The key elements needed to achieve this were the detection of a torsional signal from the cantilever and an algorithm that could correct for both tip-bending and tip-geometry. An example of image data and analysis from this system is shown in Fig. 2 from [16].

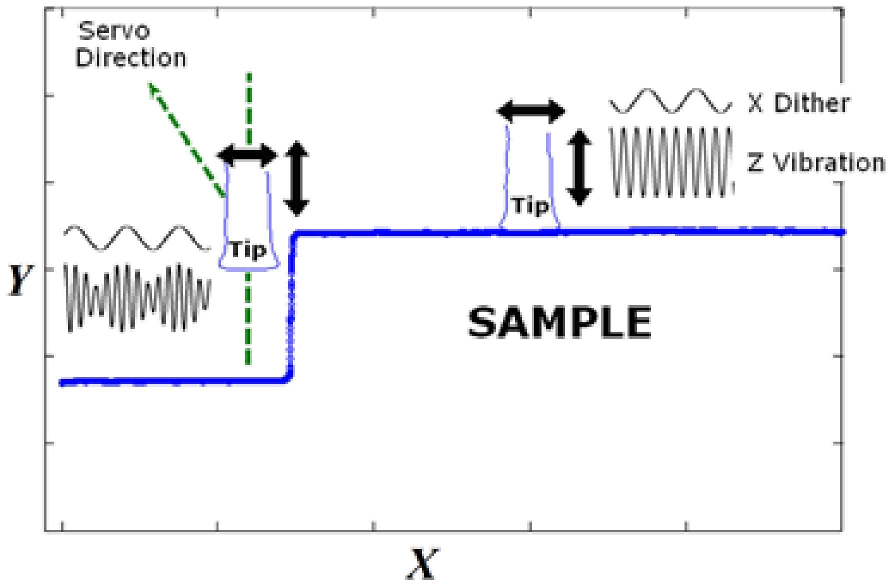

Figure 1: Schematic diagram of the CD-AFM operation. The tip vibrates in the Z direction and dithers in the lateral direction. The tip tracks both the vertical and lateral surfaces by adjusting the servo direction when a change in slope is detected by the sensor.

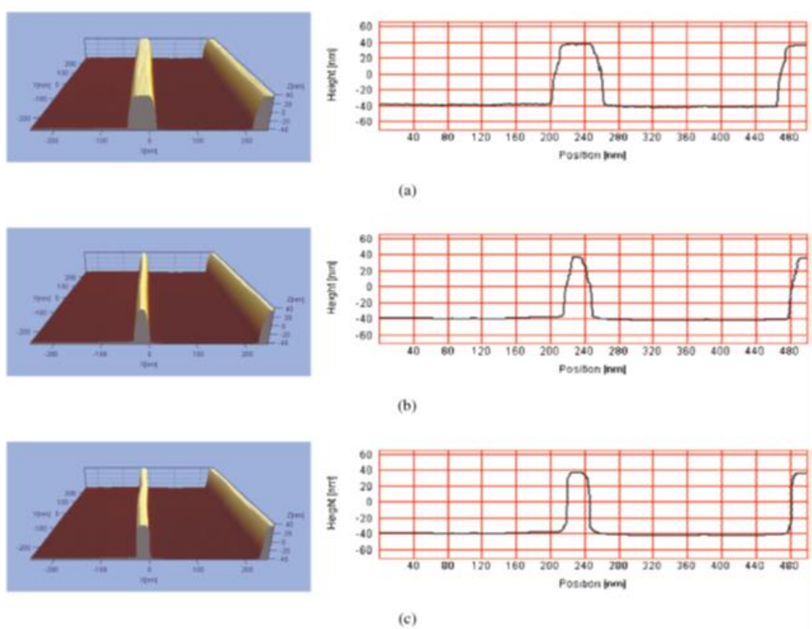

Figure 2: 3D image and cross section of CD reference sample with a poly-silicon line and SiO2 base. (a) AFM raw profile. (b) Profile with only probe shape correction. (c) Profile with probe shape and tip bending correction. (*Image used with permission[16]*)

More recently, a competing technique has been developed based on controlled and measured tilting of an AFM head during imaging [17]. This method does not require flared tips or a non-vertical oscillation of the cantilever. However, its accuracy is dependent upon the decoupling of the lateral and vertical scanner axes and the accuracy of the data stitching when the AFM head is at different tilts. In principle, this technique has the potential to play an important role in metrology applications. A basic summary of how the method is applied to the data is shown in Fig. 3 from [17].

Although it is not a commercially available technology, the national metrology institute of Germany, Physikalisch-Technische Bundesanstalt (PTB), has also developed a 3D-AFM method based on vector-approach probing that can use flared tips and has imaging capability broadly similar to CD-AFM [15]. It operates by sensing lateral deflections of the cantilever, in a manner broadly similar to lateral force microscopy, but uses a more sophisticated method of tip position control. The vector approach probing method is illustrated in Fig. 4, reprinted from Dai et al.[18] .

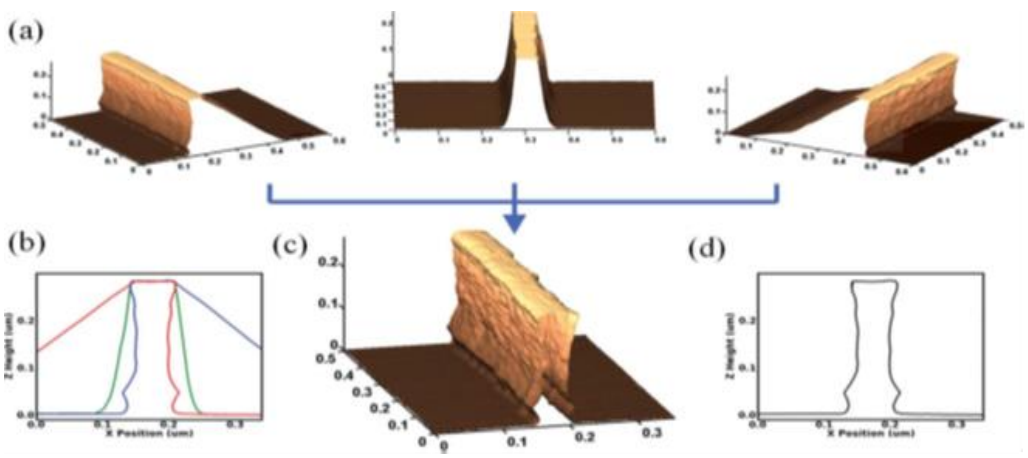

Figure 3: (a) 3D-AFM image obtained at -38◦, 0◦, and 38◦ head tilts. (b) Cross-sectional profiles, showing how the images are combined to reconstruct the 3D image. (c) 3D rendering of the reconstructed image. (d) A cross-sectional profile of the reconstructed image. (*Reprinted with permission from[17]. Copyright [2011], AIP Publishing LLC.)*

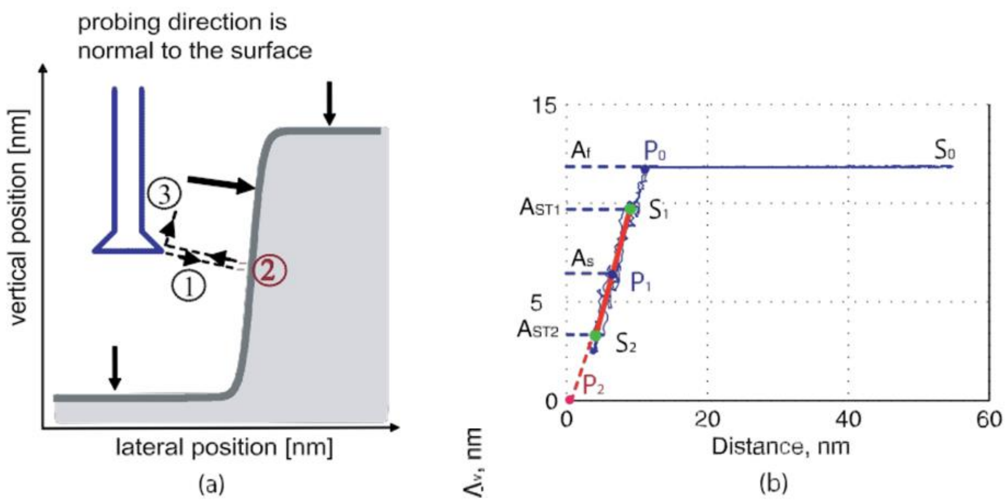

Figure 4: (a) Principle of the vector-approach probing and (b) a typical probing curve. (*Image used with permission [18]*)

1.3 Semiconductor Dimensional Measurements

The International Technology Roadmap for semiconductors (ITRS) Metrology chapter [19] lists control of complicated 3D structures such as finFETs (fin-based Field Effect Transistors) and 3D interconnects as difficult measurement challenges. The relatively tight specifications on critical dimensions, height, sidewall angle, and pitch of these features, and the need for full profile information, mean that 3D-AFM would be used in some capacity to do these measurements. This would either be as the only tool, or used in conjunction with other instruments.

The ITRS specification for printed physical gate length variability control is 1.6 nm for 2016, and 0.7 nm for 2025. Thus, the tools needed for these measurements have to perform significantly better than the specifications. It also means that calibration methods needed to verify this level of performance have to be in place before then. Table 1 shows ITRS specifications for some gate and finFET uncertainty requirements. Apart from 2015, each year until 2025 has parameters coded in red, indicating that no manufacturable solutions are known. This means that, if solutions are not developed by the specified dates, associated performance goals would not be met. Although 3D-AFMs have the capability of including other contrast modes, the demand for such implementations has not been great. This could change, however, with the advent of finFETs and other advanced devices.

The introduction of finFETs [20] increases the number of semiconductor dimensional measurements that require three-dimensional information. Unlike traditional two-dimensional planar gates, finFETs are three dimensional fins on top of the silicon substrate adjoining the gate. The benefits of finFETS include complementary metal-oxide semiconductor processing compatibility, excellent short channel effect immunity, improved current flow control, and faster switching between the “on” and “off” states. From a dimensional metrology point of view, this increased performance also means additional parameters to measure and control. Figure 5(a) shows a schematic diagram of a series of patterned lines with some of the dimensional parameters labeled. Apart from height and pitch, all the parameters listed require information from at least 2 axes. Figure 5(b) shows a traditional planar transistor, and figure 5(c) a three-dimensional tri-gate finFET. Figure 5(d) shows a cross-sectional diagram of the 22 nm process fins introduced in 2011 by Intel Corporation, and figure 5(e) the 14 nm process fins introduced in 2014. The observed performance improvements for finFETs are only possible with good variability control of key parameters. Some of these parameters, which are inherently 3D in nature, require not only 3D measure capabilities but also atomic level resolutions. The ITRS uncertainty specifications are 0.3^{o} for sidewall angle, 0.5 nm for fin height, and 0.9 nm for gate height for 2016.

In addition to new complex 3D shapes, other techniques such as directed self-assembly, multiple patterning, and smaller pitches pose challenges to CD, height, pitch, sidewall angle and defect measurements[21]. Smaller pitches mean that for electron beam-based measurements, the signal response may not be sufficiently isolated to resolve a single edge. For scanning probe-based techniques such as 3DAFM, available tips may be too large to penetrate the full depth of trenches or dense lines. CD-AFM tips fitted with carbon nanotubes[22] have been proposed, but requires addition research and development. Other measurement challenges include the metrology of contact holes, and some dimensional parameters associated with 3D interconnect metrology such as the shape of through silicon vias (TSV)[23]. Note that although 3D-AFMs may not fully measure all parameters associated with the metrology of TSV due to the large sizes involved, they could be used in conjunction with other tools to provide useful information. Broadly speaking, if a feature can be reached by the tip, and is within the limitations of tip width and working length, it can probably be measured with an AFM.

Table 1: ITRS Lithography metrology specifications for Select parameters

Year of Production	2015	2016	2020	2025
Gate (MPU Physical Gate Length)				
Printed gate CD control (nm)	1.7	1.6	1.1	0.70
Wafer CD metrology tool uncertainty (nm)	0.35	0.32	0.22	0.14
Etched Gate Line Width Roughness (nm, 3 s)	1.34	1.23	0.85	0.54
Wafer CD metrology tool uncertainty for LWR (nm)	0.27	0.25	0.17	0.11
FinFET Process Parameter Metrology Requirements				
Metrology Uncertainty for Fin Sidewall Angle (º)	0.3	0.3	0.3	0.3
Metrology Uncertainty for Gate Sidewall Angle (º)	0.3	0.3	0.3	0.3
Metrology Uncertainty for fin top corner rounding radius (nm)	0.3	0.3	0.2	0.1
Metrology Uncertainty for fin height (nm)	0.5	0.5	0.3	0.2
Metrology Uncertainty for gate height (nm)	1.0	0.9	0.6	0.4
Metrology Uncertainty for gate overhang (gate height above fin) (nm)	0.5	0.5	0.3	0.2

Manufacturable solutions exist, and are being optimized	(white)
Manufacturable solutions are known	(yellow)
Manufacturable solutions are NOT known	(red)

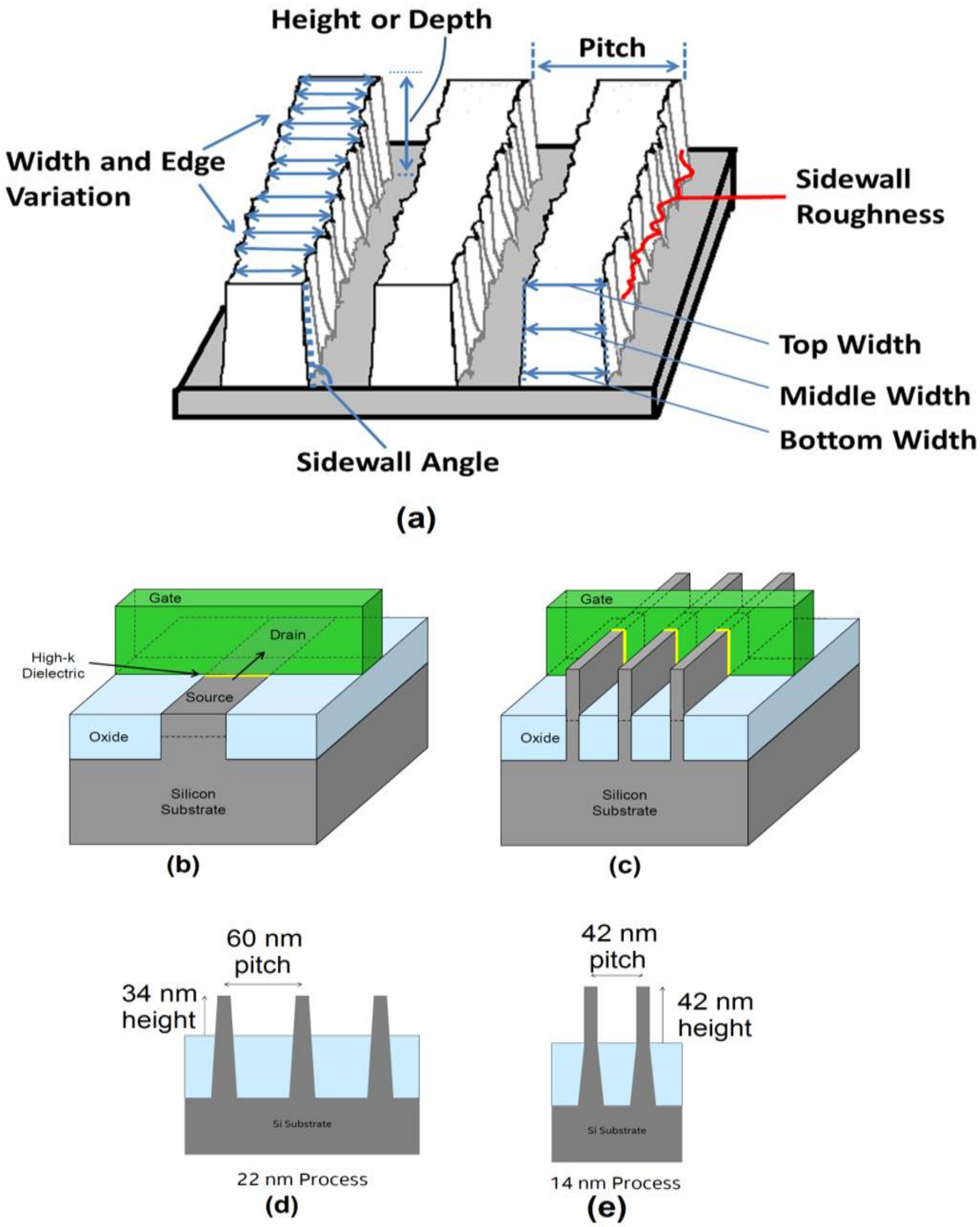

Figure 5: (a) Schematic diagram of patterned lines showing some measurement parameters (b) traditional Planar transistor, and (c) a three-dimensional trigate finFET transistor. Cross-section diagram of (d) 22 nm process finFETs and (e) 14 nm process finFETs (*Images (b) to (e) courtesy of Intel Corporation, used with permission*)

2. CHARACTERIZATION AND CALIBRATION OF 3D-AFM

2.1 Scale Calibrations

Dimensional calibration of 3D-AFM includes the type of characterization that one would perform for conventional AFMs, plus measurements utilizing aspects of the instrument that enable it to acquire 3D data. Instrument calibrations could be from first principles using methods such as displacement interferometry, where the scales are monitored by on-board displacement interferometer, or by measuring previously calibrated artifacts. Measurements using displacement interferometry provide values with traceability to the *SI* (*système international d'unités, or international systems of units*) definition of the meter through the use of a stabilized 633 nm helium neon laser. AFMs installed with this type of sensor are mostly available at national metrology institutes (NMIs) and are used to measure and certify length standards [24-29] . Most AFM calibrations are done using previously calibrated samples such as pitch and height standards. The types of characterization described below enable traceable measurements of the types of parameters shown in figure 6, which include surface roughness[30], linewidth[31], height, vias, pitch and sidewall roughness, and cover a wide range of industry relevant samples.

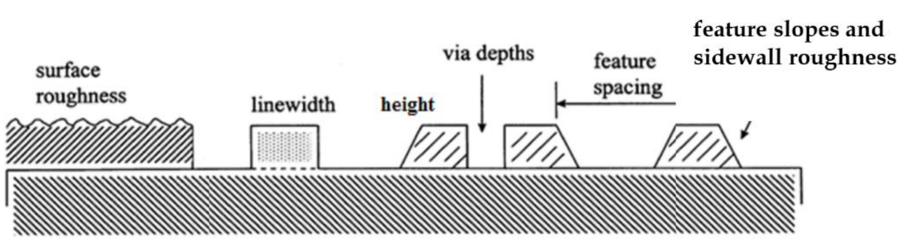

Figure 6: Key Measurands (*Image courtesy of T.V. Vorburger, NIST*)

In AFMs, magnification calibration consists of accurately characterizing the displacements of the scanner in all three axes. This is normally accomplished by using known height and pitch samples to calibrate the vertical and horizontal scales of the instrument, respectively. Although specific calibration procedures vary by manufacturer, the procedure includes the following steps

1. Evaluate the response of the displacement sensor with respect to actuator inputs.
   This involves initial measurements to determine if the calibration is off, and by how much.

2. Adjust the relationship (sensitivity) between the input (intended displacement) and the output (actual displacement) using calibrated samples.
   This is the relationship between the actuator (piezoelectric scanner), and the sensor (capacitance gauges or displacement interferometry), and is the sensitivity factor that converts actuator voltages to nanometers. For commercial instruments this relationship is usually set at the factory and only relatively small changes around the initial values are needed.

3. Re-measure and see if the input (intended displacement) and the output (actual displacement) are close to an acceptable value that makes sense for your application.

4. Ensure that the intended/actual displacement relationship is linear across the instrument measurement range.

5. Account for local deviations (non-linearity) across the measurement range.
   The sensitivity of the piezoelectric scanner varies with respect to measurement range. Depending on where your sample falls within the measurement range, local variations could be non-negligible.

6. Develop an uncertainty statement about the calibration process.

Figure 7(a) gives a visual representation of the calibration process. The thin dotted line labeled as the reference line is the unity slope linking the actual and apparent displacement and comes from either the *SI* definition of length or calibration samples. For all intents and purposes, this is an ideal line. The dashed line labeled average slope is the calibration curve between the actual and apparent displacements. The difference between the two slopes is the scale calibration offset to be corrected. The spread of the calibration values is represented by the curved dashed lines. As shown by the plot, although the average curve could be linear with respect to the overall measurement range, there are local slope variations at different portions of the measurement range. This is one of the reasons why it is important to use calibration samples whose sizes are close to those of the features being measured. In addition to scale errors, there could also be rotation around the principle axes. These are shown in Figure 7(b). They represent angular deviations as the stage moves one point to the other. Examples of scale calibration of AFMs can be found in Orji et al.[14, 32] . In the rest of the section, we focus on specific calibrations for 3D-AFM.

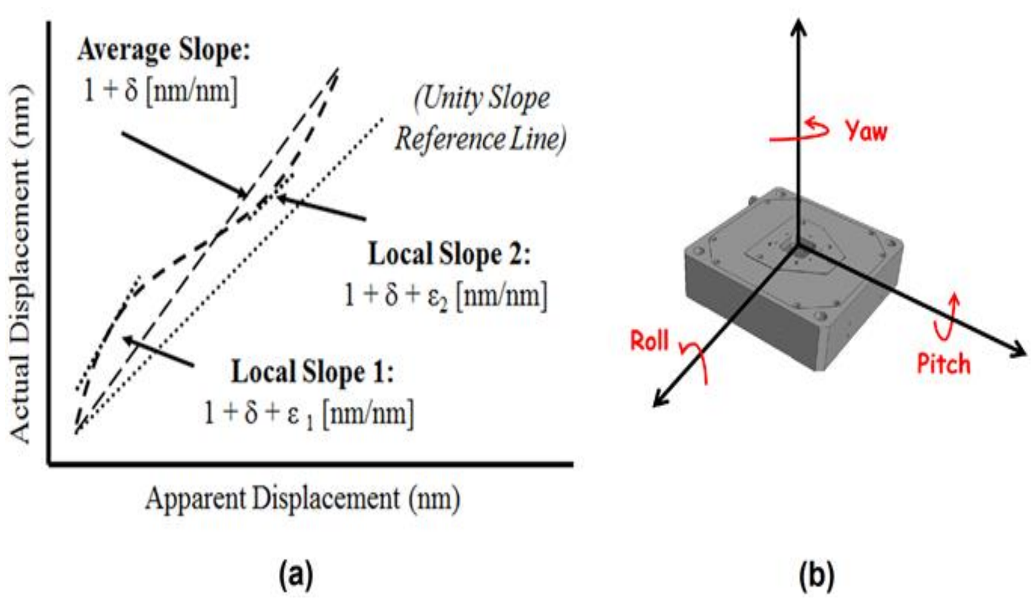

Figure: 7 (a) Model of scale uncertainty and non –linearity terms in displacement measurements (b) Rotational errors around the main axes of the scanner.

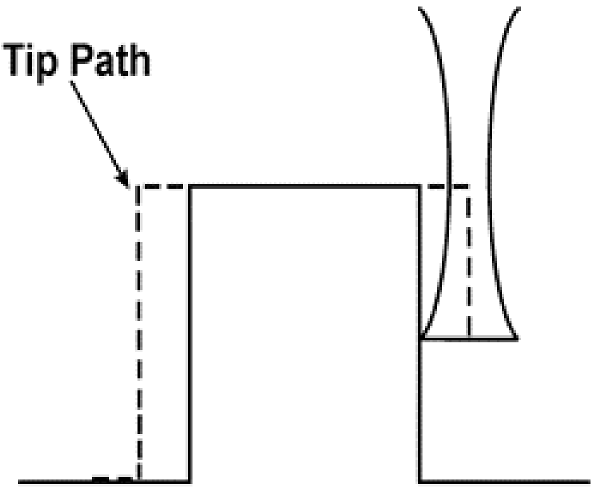

Figure 8: Schematic diagram of a 3D-AFM flared tip scanning over a feature. The image represented by the tip path is a dilation of the feature by the tip.

For 3D-AFMs, the main operational difference with respect to conventional AFMs is the ability to acquire data in more than one axis, specifically by accessing feature sidewalls. So, the extra element that needs calibration is the tip/sidewall interaction.

Note that for width measurements, lateral scale calibration is not enough. Local geometric distortions caused by the finite size of the tip mean that AFM images are dilations of the sample and tip. So, removing tip information is essential to obtaining accurate results. Figure 8 shows a schematic diagram of a flared 3D-AFM tip scanning over a feature. The apparent image as shown by the tip path includes the tip-width. To determine the size of the feature, the tip-width should be known a priori. The main technique to determine tip-width is the use of artifacts calibrated using transmission electron microscope (TEM)[33-36] .

2.2 Calibration Sample Characterization.

The most accurate methods used to calibrate 3D-AFM tip width derive traceability through detection of a crystalline lattice spacing. The first step is to identify suitable crystalline samples and processing/fabrication methods capable of producing vertical sidewalls [36-39]. In one of the implementations

[37], the starting material was a {110}silicon-on insulator substrate. The reference features are aligned with the <112> vectors, with the (111) plane forming the sidewall of the features. The sidewalls, which are preferentially etched, have a 90-degree angle. This is important because it provides a uniform feature width from the top to the bottom of the sample. A series of widths that span the intended range of measurement sizes are usually fabricated, which can be valuable in calculating the linearity of the calibration process. Figure 9 shows a schematic of a series of features used for calibration [37]. In this example, all the features are aligned on one sample, so they can be measured and cross-sectioned under the same condition. The samples are measured with the 3D-AFM under the same conditions, and a subset is cross-sectioned and imaged using a method of TEM capable of resolving the lattice spacing: either high resolution TEM (HRTEM) or annular dark-field scanning TEM (ADF-STEM).

Figure 10 shows a representative image of the HRTEM micrograph. To facilitate counting, the lattice positions are imaged as lines rather than atoms. This is done by slightly tilting the sample along the axis of the (111) planes. Figure 11(a) shows an ADF-STEM micrograph of a line feature, and figure 11(b) the corresponding line plot. Each peak in the line plot corresponds to a lattice position. Some of the uncertainties associated with using TEM images for this type of calibration are evident in figure 11. The lattice positions close to the edge are usually difficult to resolve. The roll-off or curvature at the edges of the feature in figure 11(a) is caused by spherical aberration in the optics. After evaluating the data and developing an uncertainty budget, the results are used to adjust the values of the remaining samples in the calibration group. An uncertainty evaluation is performed for the 3D-AFM measurements, and the samples are ready to be used. To ensure that the calibrated values are not drifting, a procedure to periodically monitor the sample for damage should also be developed. The reference lattice spacing does not have to be from the line itself. Figure 12 shows a TEM micrograph from Tortonese et al. [34], where the lattice spacing reference is off to the side of the line feature. Both images have the same scale, so the reference is applicable to all the features in the image.

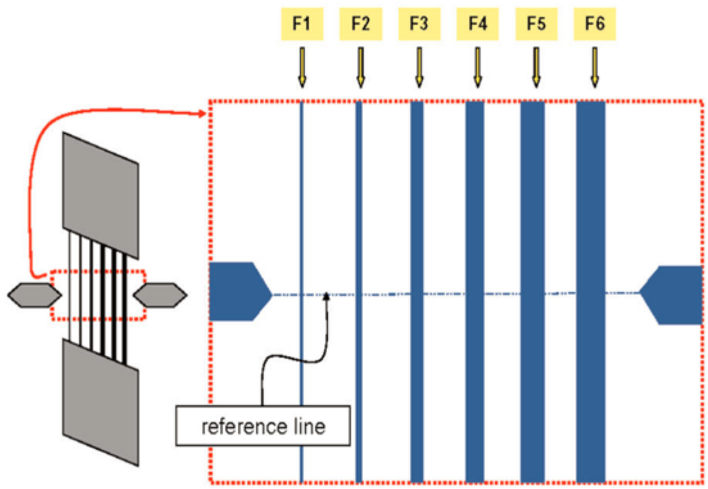

Figure 9: Schematic Diagram of a lattice-based calibration sample. The features labeled F1 to F5 are cross-sectioned at the reference line and imaged with HRTEM.

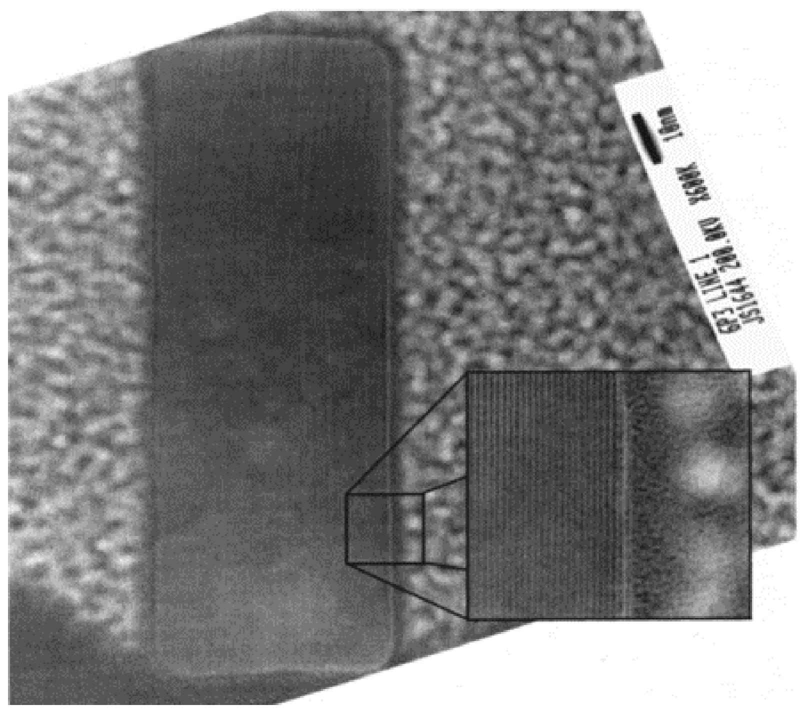

Figure 10: Negative of the high-magnification 400k HRTEM image of the narrowest feature used. At this magnification, the silicon lattice fringes are visible as can be seen in the enlarged portion of the sidewall shown in the inset.

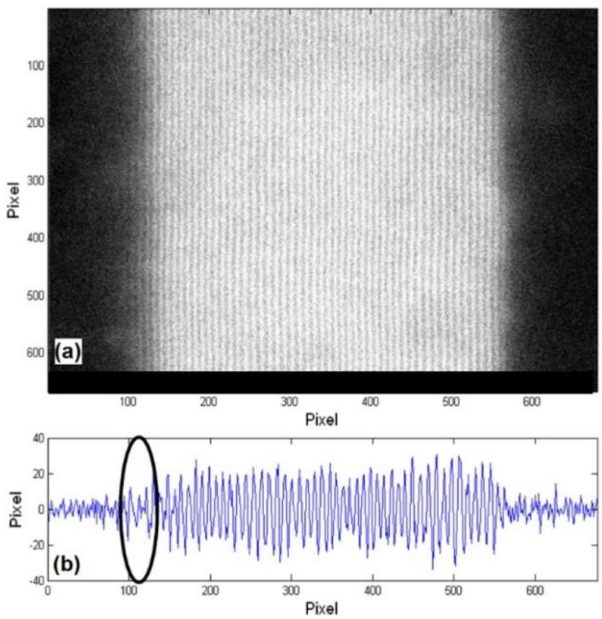

Figure 11: (a) ADF-TEM image of a SCCDRM feature. The roll off at the left edge of the image could be due to aberration in the optics. (b) A profile of the center location of the ADF-TEM image. The questionable edge locations are highlighted. To enhance signal to noise ratio, the above profiles are produced by averaging five scan lines.

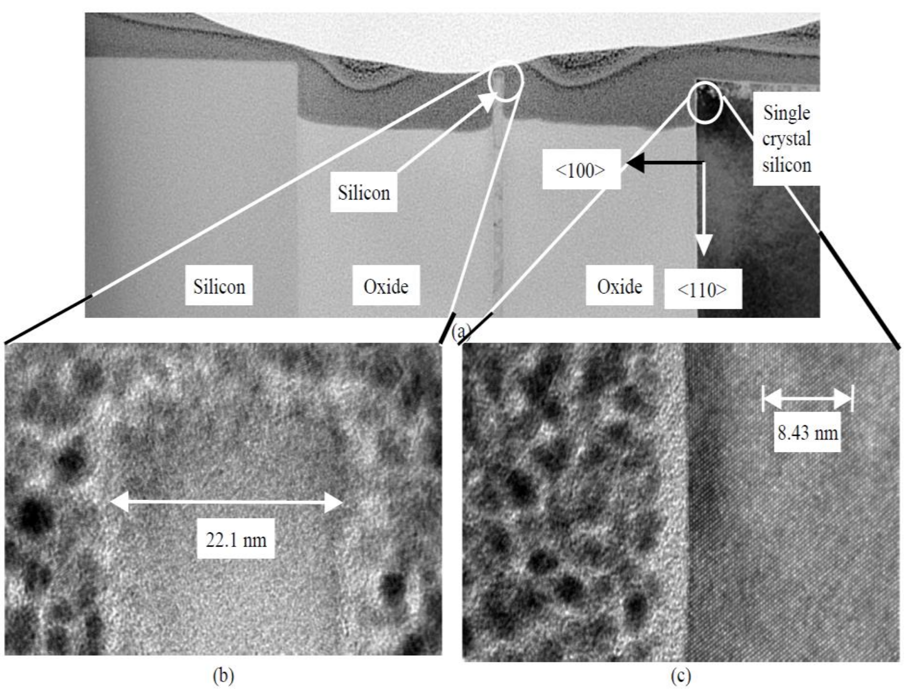

Figure 12 (a) TEM images of a line feature. These images were used to measure the (b) close up view (c) silicon atomic lattice spacing reference for the line feature. (Image from Tortonese et al. [34], used with permission)

2.3 Tip-Width Calibration

The calibrated samples described above could be used on a day to day basis or transferred to other samples for regular use. Figure 13 shows profiles of flared CD-AFM tip and associated parameters. The main parameters are width, effective tip length, vertical edge height and tip overhang. The procedure for width verification is shown in figure 14, where TW represents the tip width, and CW and AW represent the calibrated width and apparent width, respectively. The primes indicate known quantities. After measurement, the calibrated width is subtracted from the apparent width to get the tip width. In addition to tip-width, the shape of the tip can also be determined. A sharp spike or overhang with a radius of less than 5 nm is measured, and using mathematical morphology or a mathematically equivalent analysis, the shape of the tip can be reconstructed [13, 40, 41]. Figure 15(a) shows a profile of a silicon overhang characterizer sample (SOCS). The TEM image in figure 15 (b) shows an edge radius of 2 nm for the SOCS. Another widely used shape characterizer is the flared silicon ridge characterizer shown in Figure 15(c). In addition to tip-width calculation, error due to higher order tip effects [41-43] can also add to the uncertainty. In state-of-the-art 3D-AFMs, tip width and shape verification measurements are usually automated.

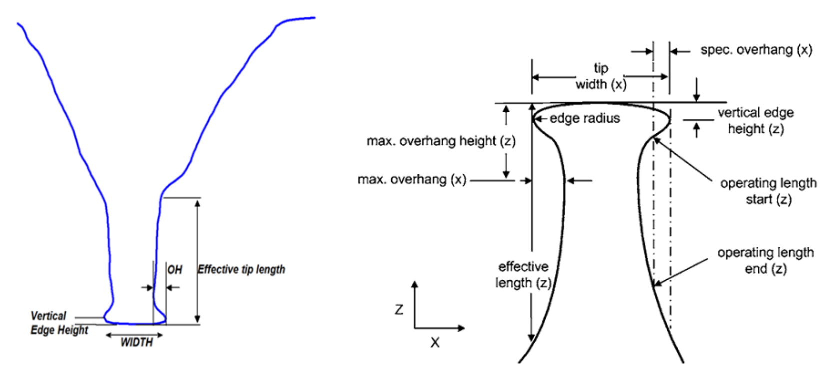

(a) Flared 3D-AFM tip **(b) Flared 3D-AFM tip shape parameters**

Figure 13: Profiles of (a) flared CD-AFM tip (b) close-up of flared CD-AFM with shape parameters. (*Image (b) reprinted with permission from[13]. Copyright [2005], AIP Publishing LLC.)*

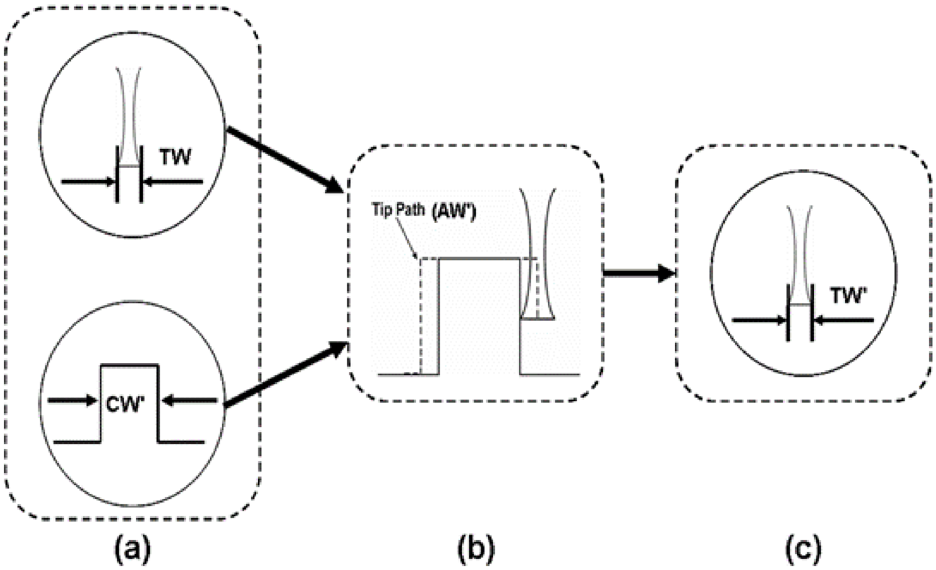

Figure 14: Schematic diagram of the width determination process for flared 3D-AFM tips. The primes indicate known quantities. (a) The tip width (TW) is unknown but the width of the tip calibration structure (CW) is known. (b) The apparent width AW produced by CW and TW is known. (c) CW is subtracted from AW to get TW. For measurements of linewidth, the process is reversed.

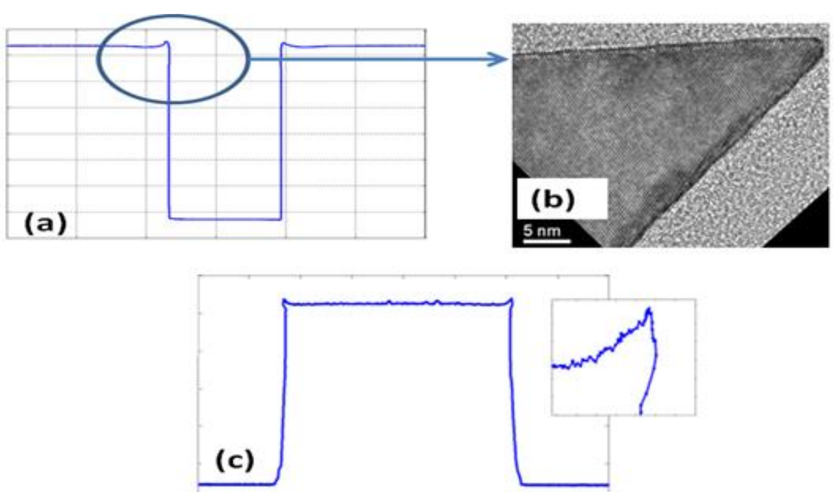

Figure 15: (a) Profile of a SOCS. (b) TEM image of the sharp edge of the SOCS. The sharp points are less than 2 nm in radius. (c) Profile of a flared silicon ridge.

2.4 Angle Verification

Broadly speaking, three-dimensional shape could be regarded as a succession of surface and sidewall segments with varying angles. So, it is important to know if the instrument is providing consistent and accurate angle information. The approach described below is more of a verification procedure rather than a calibration exercise. Unlike vertical or lateral calibrations, the response function of the scanner is not adjusted. Given that angular measurements ultimately consist of lateral and vertical scanner displacements, the verification process fundamentally rests on an accurate calibration of the instrument scales. One of the most important angle verification checks is to find out if the head is misaligned with respect to sample lateral axis, and by how much. Any misalignment if not accounted for, will be included in all angle measurements. Figure 16 shows a schematic diagram of a technique known as image reversal, used to check for misalignment. The AFM cantilever in the diagram is measuring the same feature, but in different scan direction and sample orientations. If the instrument's head is normal to the sample surface, each sidewall should have the same angle in spite of the measurement orientation. Some instruments (or cantilever set-ups) have an included angle in one scan axis, this should be corrected before obtaining the final result. The actual angle verification is rather straight forward and involves the following familiar steps

1. Measure a series of angles with 3D-AFM within the desired range.
2. Cross-section a subset of the samples, and confirm the results with TEM or cross-section SEM (depending on the size of the features)
3. Adjust the results and develop an uncertainty budget.
4. Keep some of the calibration samples for periodic checks

Figure 17 shows a collection of TEM micrographs of features used to verify angle for a 3D-AFM [10]. The angles and feature sizes should be representative of those used for routine measurements. Figure 18 shows results from an angle verification exercise. The "calibration" curve shows close agreement between the cross-section samples and TEM. The artifacts with the smallest residuals were preferentially etched along specific lattice planes, ensuring a consistent value across the sample.

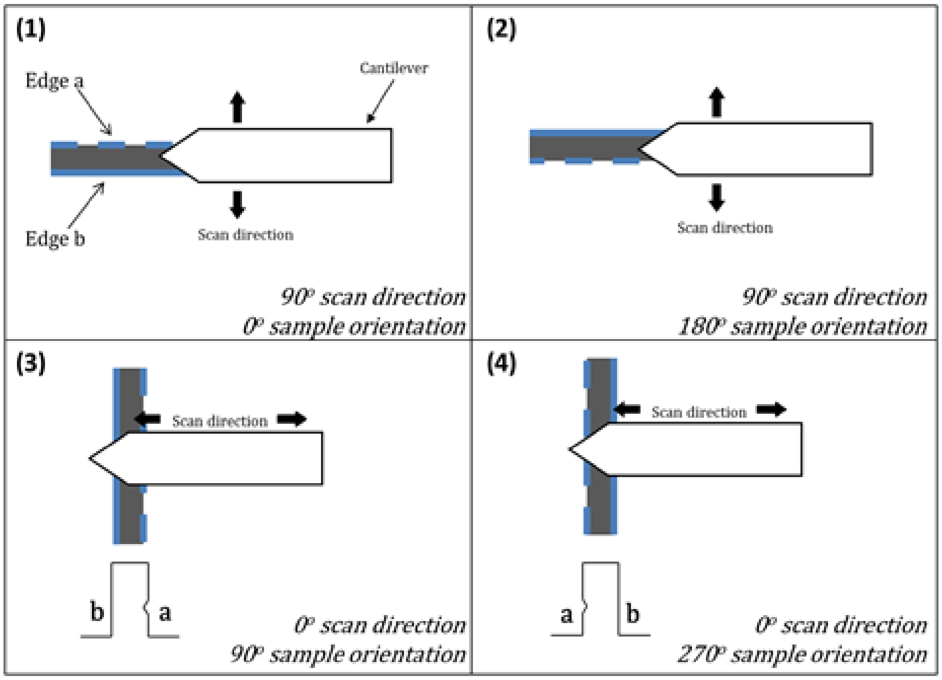

Figure 16: Image reversal technique. The sidewall angle for each edge should be the same irrespective of how it is measured. Any sidewall angle difference with respect to scan direction means that the head is tilted and should accounted for depending on the measurement.

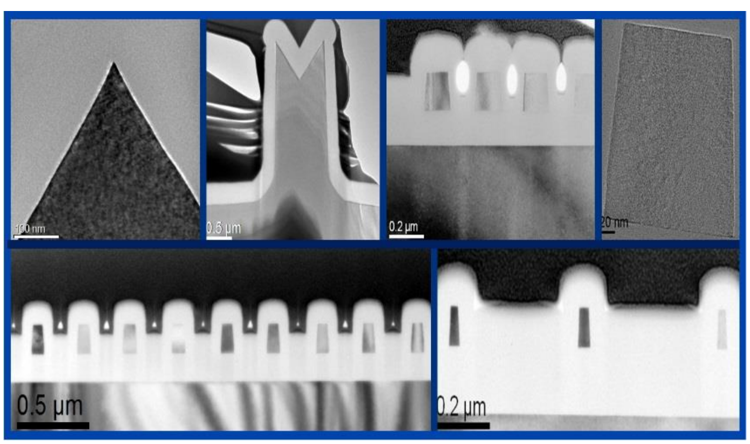

Figure 17: A collection of artifacts used to verify angle measurement capability (From Orji et al. [10])

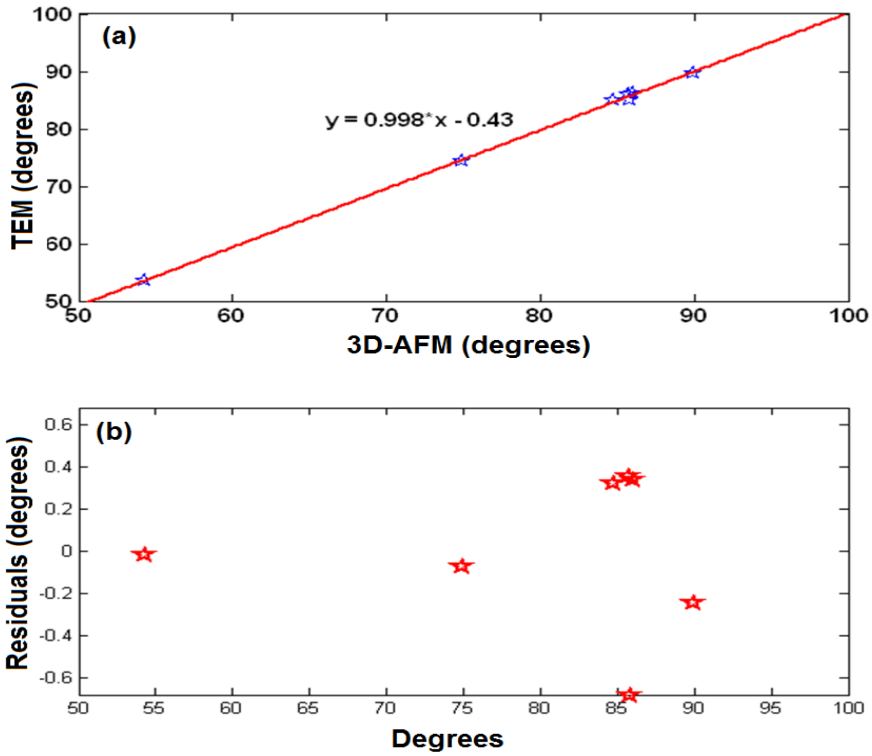

Figure 18: (a) “Calibration” curve for TEM and 3D-AFM data (b) Residuals for the plot in (a). Artifacts with the smallest residuals are preferentially etched along specific lattice planes, ensuring a consistent angle across the sample. (From Orji et al. [10])

2.5 Uncertainty[1] and Accuracy Considerations

([1]*Here we use uncertainty broadly to mean any evaluation and analysis framework used to quantify measurement errors.)*

The uncertainty requirements for 3D-AFM depend on the desired application. Whether the purpose is routine measurements, tool and fleet matching, tool acceptance verification, reference measurement systems (RMS), or routine measurements, the goal of error/uncertainty evaluation is to ensure that results are within the required tolerance for that application. A good start is to evaluate different aspects of the instrument and establish a performance baseline. This will enable the user to determine the instrument’s capabilities and stability. Over the years different methods have been developed to calibrate and evaluate AFM measurement error [14, 32, 44-47]. Methods that are specific to 3D-AFM generally reflect the use of the instrument as an RMS or as part of a hybrid/holistic measurement approach [48, 49].

One approach that has been used over the years is the measurement linearity method. The goal is to quantify the residual error of a specific measurand when an instrument (tool-under-test (TuT)) is compared with another instrument (RMS, discussed later) whose performance is known. A regression method proposed by John Mandel [50], which includes errors in two axes is used in the analysis. An example of this approach is the total measurement uncertainty (TMU) method [44, 51]. Note that "total" in TMU does not mean that this metric captures all associated measurement uncertainties. This happens to be the name the developers called their technique. In using the Mandel approach for TMU analysis, the RMS uncertainty at each datum in the linearity curve represents the estimate of errors in one axis, while a starting point for an estimate of the uncertainty of the TuT is the precision. This is used to determine the Mandel parameter needed for fits with errors in two axes.

The definition ($TMU = 3\sqrt{\hat{\sigma}^2_{Mandel} - \hat{\sigma}^2_{RMS}}$) [51] reflects the original reference metrology TuT application of TMU. In this definition, estimates of the RMS error are subtracted from the formula to get the TMU, thus the remaining error estimate is attributed to the TuT. Broadly speaking, this method is useful for comparing the performance of different instruments, tool to tool matching or fleet matching. One drawback is that it does not identify specific error sources if additional analysis is not performed. Also, unless traceable calibration samples are

used, this procedure does not yield traceable results. The 2007 ITRS edition explicitly included measurement uncertainty in the requirements table using the formula $U^2_{combined} = \sigma^2_S + \sigma^2_P + \sigma^2_M + \sigma^2_{other}$. *S* stands for sampling, *P* for precision, and *M* for matching. *Other* refers to all remaining components including systematic and calibration errors. An example of the role of sampling using the ITRS definition is described in Bunday et al. [52]. TMU definition was modified $TMU = 3\sqrt{[\sigma^2_P] + [\sigma^2_S + \sigma^2_{other}]}$ [53] to reflect the ITRS definition.

Another uncertainty analysis approach, used at NIST [54], is to develop an estimated contribution from all known error sources for the instrument and sample. Error contributions that can be evaluated using statistical methods are known as Type A, while errors evaluated using some combination of physical models, assumptions about the probability distribution, and measured data are referred to as type B. The error from each source is applied to the measurement model depending on how it affects the measurement. For example, in linewidth uncertainty, the zeroth width tip error is additive [41, 43], while the scale factor error is multiplied by the mean value (see table 2 below). The error components are added in quadrature to get the combined standard uncertainty. This is then multiplied by a coverage factor *k* to get the combined expanded uncertainty for the measurements.

Table 2 shows an uncertainty table for linewidth measurements from a 3D – AFM [32, 33]. The type A errors are repeatability, reproducibility, and sample uniformity. Generally, type A errors will include terms that cannot be separated, but whose influence would show up as measurement variability. Type B errors include tip size, tip bending, scale factor, nonlinearity, in-sample-plane, and out-of-sample plane cosine errors. If the measurement is traceable to the *SI* through a calibration samples, the combined uncertainty of that sample is listed as type B error. Although the measurement linearity method of uncertainty analysis is widely used in semiconductor manufacturing metrology, we prefer developing estimates for each error component for following reasons:

- It isolates different error sources, and makes it easier to focus on the biggest ones.
- It explicitly includes systematic errors.
- It explicitly addresses the need for different measurement models and probability distributions (if needed). *For example, although pitch and linewidth are both lateral measurements, each requires a different model.*
- It explicitly allows handling of correlated data. *For example, although tip related uncertainties such as zeroth order, higher order effects, and tip bending uncertainties could be explicitly stated, they may not always be independent.*

Other sources of error include the lab or manufacturing environment, measurement setup and procedure, algorithms, physical constants, the definition of the measurand, and of course the metrologist among others. The key is to make sure that major sources of error for a particular measurand are known. It is also important to note that an uncertainty budget applies to a specific measurement, rather than the instrument. Although a low uncertainty could indicate a high performing instrument, it only refers to how the instrument was performing during a specific measurement. Examples of uncertainty budget development can be found in the following references [28, 32, 33]. Finally, the allowable tolerance and overall purpose of the measurement will ultimately determine how much effort should be spent on uncertainty analysis.

Table 2: Example Uncertainty Table for Linewidth Measurement

Type A	
Repeatability, reproducibility, sample uniformity	0.4 nm
Type B	
Tip	
Zeroth order	0.8 nm
Higher order	0.51 nm
Scale factor (linear term)	$1 \times 10^{-3}\ W$
Nonlinearity	$2.44 \times 10^{-4}\ W$
In-sample-plane cosine error	$0.15 \times 10^{-5}\ W$
Out-of-sample-plane cosine error	$0.15 \times 10^{-3}\ W$
u_C (Width) $= [(1\ \mathrm{SD})^2 + (0.95\ \mathrm{nm})^2 + (1.04 \times 10^{-3}\ W)^2]^{1/2}$	

[a] Note. W is the width in nm.

(*Table 2 from Orji et al. [32]*)

3. APPLICATIONS OF 3D –AFM

Application of 3D-AFM in semiconductor measurements fall under two broad categories. The first is measurements of specific parameters. These include linewidth, height, sidewall angle, and full three-dimensional profiles of different types of features. The second one is where the instrument is used to introduce or verify measurement accuracy, and or used in combination with other instruments in a hybrid or complementary way. The difference between these applications is subtle. In the first instance the focus is on what is being measured. Here the instrument is used because of its capability to measure three dimensional features. The second instance is about how the results are being used. In this instance, it is used to introduce or verify relative or absolute accuracy or used in a hybrid or complementary way with other instruments. When used as part of a hybrid measurement, each instrument either measures only parameters it is most suited for or where it yields the lowest uncertainty. Note that even in the second example, the actual parameters being measured are the same as in the first instance. Figure 19 shows a finFET feature with multiple parameters such as height, width at different heights, and sidewall angle among others. A full three–dimensional profile of this feature will require measurement and extraction of multiple parameters.

The key benefit of using the 3D-AFM is the ability to obtain full 3D profile in one measurement. Three more applications – contour metrology, hybrid or complementary metrology, and reference measurement system, are described below. These examples are meant to highlight different measurement strategies rather than specific parameters. As indicated above, if a feature is within the limitations of tip width, working length, and can be reached by the tip, it can be measured.

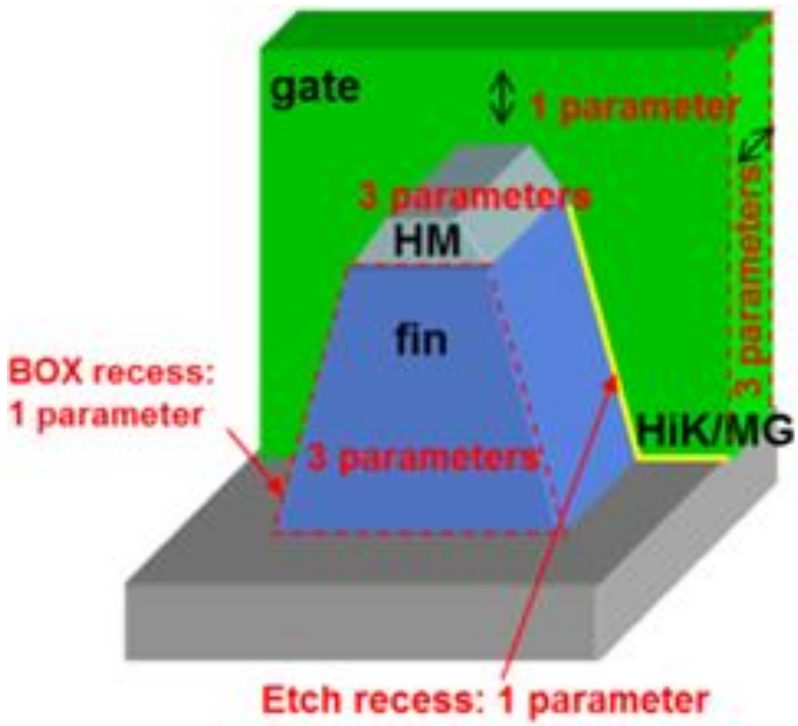

Figure 19: Schematic diagram of a three-dimensional feature, showing a basic unit cell of a finFET. A total of twelve parameters are shown (*Image courtesy of Benjamin Bunday, SEMATECH. Used with permission[21]*)

3.1 Reference Measurement System

A key application of 3D-AFM is as a Reference Measurement System (RMS). Broadly speaking, many of the dimensional measurements in semiconductor manufacturing are not traceable to the *SI* unit of length. There is greater emphasis on precision and tool matching rather than absolute traceability. In addition, the fast pace of development has often made it difficult to introduce standards in a timely manner. A well characterized instrument that could measure a wide range of parameters of interest could be used as a way to introduce traceability (or consistency) to the measurement process. For critical dimension measurements, the main instrument used for in line process control is the scanning electron microscope (SEM). Although SEMs have very high throughput, SEM measurements of size can be sensitive to the material properties of a feature in addition to its geometry, and proximity to other features. Consequently, two features of the same geometric size but different material composition could exhibit different apparent widths in SEM measurements. Achieving consistent results across such different materials would require good models of beam sample interaction physics for each material and measurement condition. In a manufacturing environment where measurements are made at multiple stages in the process, this is often not practical.

The 3D-AFM provides measurements that are relatively insensitive to material properties, has sidewall information along the primary axis, and can be traceable to the *SI* meter. Several examples of a CD-AFM based RMS include work by Banke and Archie [44]; Marchman[46]; Ukraintsev and Banke [47]; Bunday[55, 56]; and Clarke et al.[57] among others. Figure 20 shows a schematic diagram of a RMS as implemented by NIST in collaboration with SEMATECH [32]. In this implementation, the RMS is represented by a 3D-AFM that is calibrated for height, pitch, and width with samples traceable to the *SI* meter. The 3D-AFM is then characterized with these samples, thereby lending traceability to the instrument[58]. Note that the samples do not need prior calibration if the instrument has intrinsic traceability such as displacement interferometry. The 3D-AFM is then used to characterize a set of wafers and artifacts which is used to evaluate a faster inline tool. So, measurements that are made with the inline tool will be traceable to the *SI* meter through the characterized samples, the 3D-AFM, and the initial calibration sample. Figure 21 shows a schematic diagram of the traceability of the CD-AFM RMS to the *SI* meter. CD-AFM

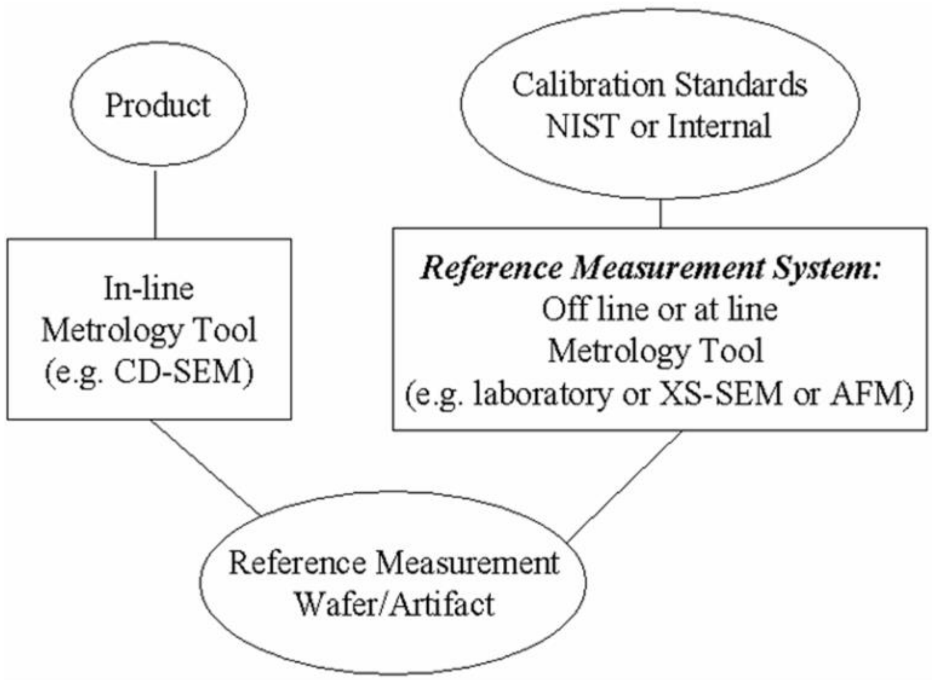

Figure 20: A conceptual diagram of the reference measurement system. The reference measurement wafer or artifacts connect the RMS instrument with the inline tools. CD-SEM stands for critical dimension scanning electron microscope, and XS-SEM for cross-sectional scanning electron microscope.

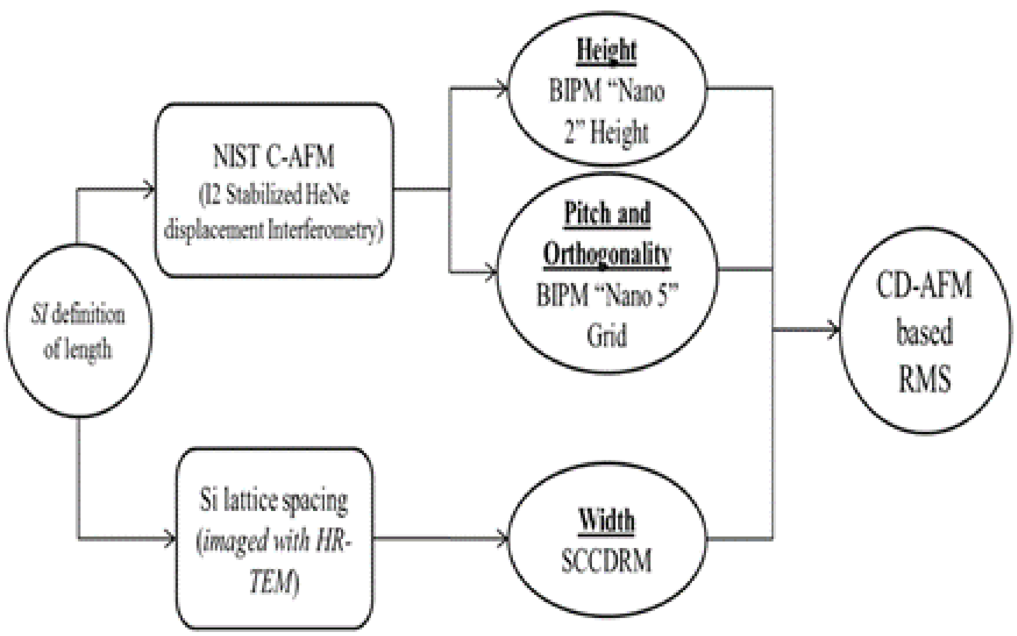

Figure 21: Schematic diagram CD-AFM based RMS traceability.

3.2 Contour Metrology

Contour metrology is a way to verify that the layout of features in the wafer plane prints as intended. It is an important element of a set of techniques known as optical proximity correction (OPC) methods in lithography models [48, 59-64]. The use of OPC, which is a resolution enhancement technique for optical lithography, is necessitated by the continued decrease in feature sizes, and the need to print small features with large wavelength photons in deep sub-wavelength regime. As lithographically printed features get smaller, specific designs may not print as intended. This is due to optical proximity effects caused by limitations of the lithography tools. To compensate for this error, an OPC model is used. This involves using starting designs that are different from the intended outcome, but will result in the required designs once they are printed. The actual model development requires knowledge of the lithography equipment, process, and materials. To ensure that the final features have the intended shapes (or profiles), they have to be verified using metrology tools. Contours provide a relatively fast way to verify to the OPC models.

The 3D-AFM has been proposed as an instrument for contour measurement and verification [61-64]. The use of 3D-AFM will enhance the overall quality of the contour information by providing accurate width information used to extract the contours. In addition, the data could also be used to provide a full 3D profile that is traceable to the *SI* meter. Although CD-AFM data has a three-dimensional structure, the planar two-dimensional data required for contour metrology is not easily extracted from CD-AFM data. This is due primarily to the limitations of the CD-AFM method for controlling the tip position and scanning, in which the relevant sidewall data is only obtained in one lateral axis. A technique for extracting contours from 3D–AFM is outlined in [63]. It involves using two images of the same features acquired with orthogonal scan axes of the instrument. As mentioned above, the 3DAFMs have a designated fast scan axis. This is the measurement axis where the dithering tip makes “contact” with the sidewall. This means that features in the same image, whose sidewalls are not in the measurement axis would not be imaged correctly.

Figure 22 (a) shows images of the same feature acquired using two orthogonal axes. A closer look at the images shows that there are no data points on the feature sidewalls that are orthogonal to the fast scan axis, which is labeled as the scan direction in the images. This absence of information is due to the lack of lateral tip-sample feedback and position control along the slow scan axis. The solution is to extract contours from both images and stitch the profiles together. Figures 23(a) and 23(b) shows the extracted profiles from each image in figure 22. Figure 23(c) shows SEM images of the same feature, and figure 23(d) contours extracted from the SEM images overlaid with contours extracted from two CD-AFM images. Depending on the application, they could be filtered and then compared with contours from SEM or graphic database system file. The benefit of using the 3D-AFM for contour metrology is not only for its sidewall access, but to introduce traceability to the data.

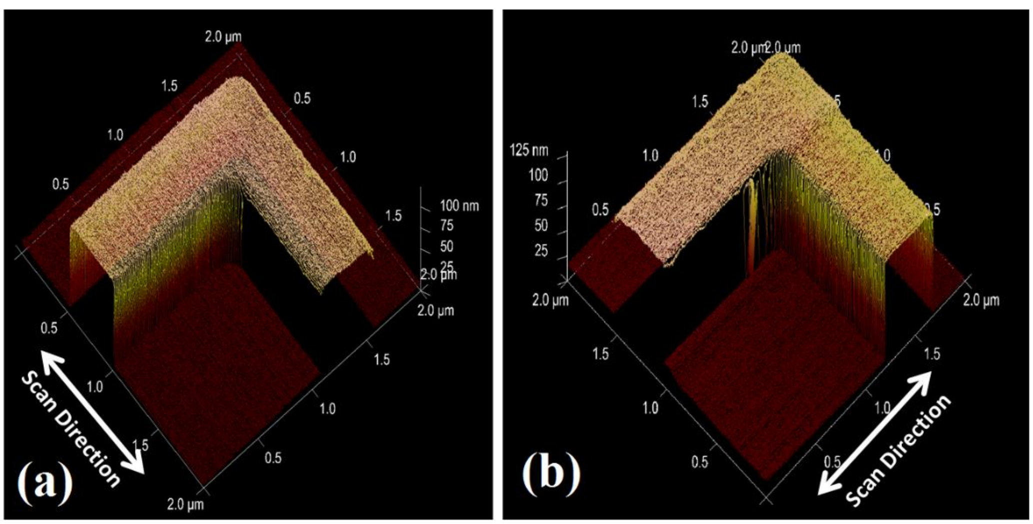

Figure 22: CD-AFM images of the same feature taken at different scan directions. (a) The image was acquired with the tip scanning along the x-axis. (b) Image acquired with the tip scanning along the y-axis. Note the complementary regions of missing data in both images. Feature sidewalls that are mostly black for image (a) are mostly filled in for image (b) and vice versa.

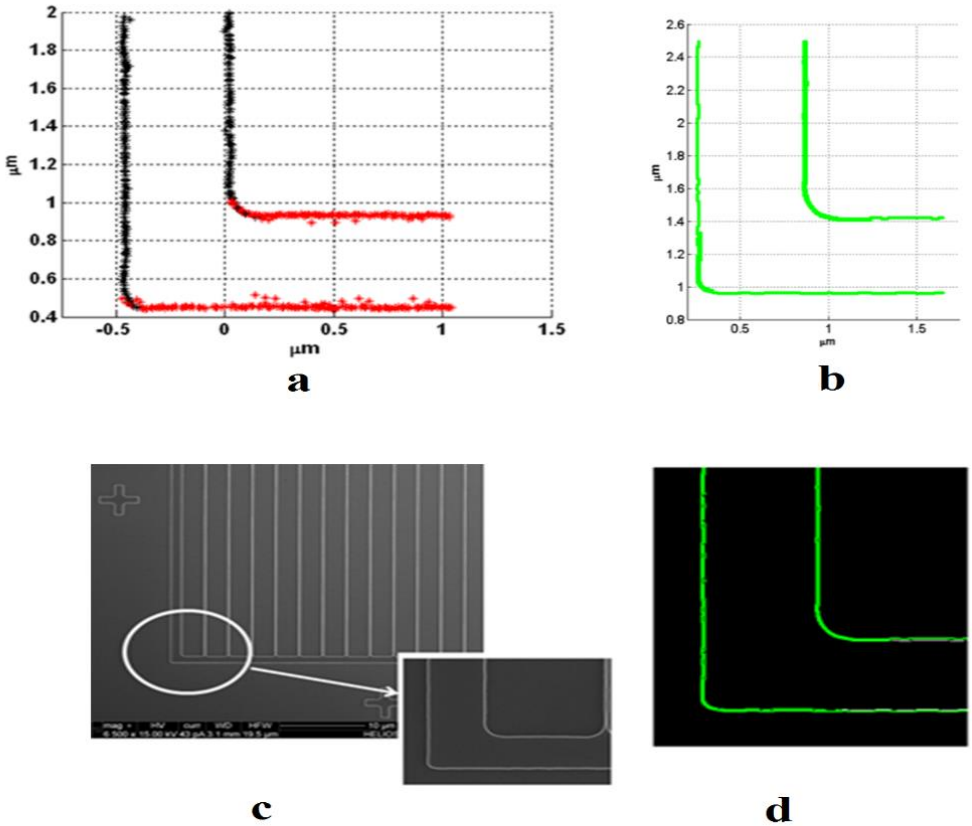

Figure 23: (a) Raw contours extracted from CD-AFM images to form a composite contour profile. (b) Fits extracted from the profile in (a). The tip width is accounted for in the fitted lines. (c) SEM images of the same feature, (d) contours extracted from the SEM images overlaid with contours extracted from two CD-AFM images.

3.3 Complimentary and Hybrid Metrology

The premise of hybrid metrology is that for some measurements no single instrument has the capability, resolution, speed, or low levels of uncertainty needed to characterize all the parameters. This means that at least two or more instruments would be used, and the results combined to get the final answer. This technique has also been referred to as holistic metrology. Figure 24 shows a conceptual diagram of hybrid metrology. Each instrument provides information on the measurand or parameter that it is most suitable to measure. In the example in the diagram, which is for linewidth, line-to-line variation information is obtained from the SEM and AFM, shape information from CD-SAX, and average CD information from multiple sites are provided by the optical critical dimension (OCD). This is used to develop a generalized model of the measurement. The role a specific instrument plays within a hybrid metrology ensemble depends on the measurand, the specific measurement model, and what the measurement is going to be used for. Model development usually involves the use of Bayesian statistics (where the values are treated as a priori information), parallel regression or both. A major consideration is how to combine the results in a consistent and error-free way. One possible problem is methods divergence. This is where different measurement methods produce different results for the same nominal measurand [65]. This could be due to the probe-sample interaction physics, the definition of the measurand, or the analysis algorithm among other things. For example, the probe-sample interaction of an AFM (cantilever and tip), SEM (electron beam), CDSAX (x-rays), OCD (optical beam) are all different, and a comparison among the results must take into account the uncertainties involved in modeling the response function of each instrument. Note that the main difference between RMS described above and hybrid metrology is the relationship between the instruments.

In hybrid metrology, each instrument is better suited for a specific measurand, but may not necessarily derive their traceability from the group. Figure 25 and table 3 show some results from hybrid metrology measurements from Zhang et al. [66]. Figure 25 shows reflectivity curves and fits from patterned nitride lines on polysilicon measured with OCD. The curves represent four combinations of scan direction and orthogonal linear polarizations for trapezoidal shaped lines. The data is evaluated for top width, middle width, bottom linewidth, line height, and the percent variation of the optical constant n. A Bayesian statistical approach is used to combine the results with a priori AFM measurements of the same features. The results in table 3 show that when AFM results are included in the regression model, the uncertainties are lower. Essentially, the AFM results for some of the parameters are embedded in the optical regression model, and the uncertainties provide a smaller floating range for the parameters involved. A detailed description of the Bayesian approach, regression model, advantages and limitations are contained in Zhang et al. [66]. Other examples of hybrid metrology implementation include [48, 49, 66-69]. A collection of papers on hybrid and holistic metrology can be found in a special section edited by Vaid and Solecky[69].

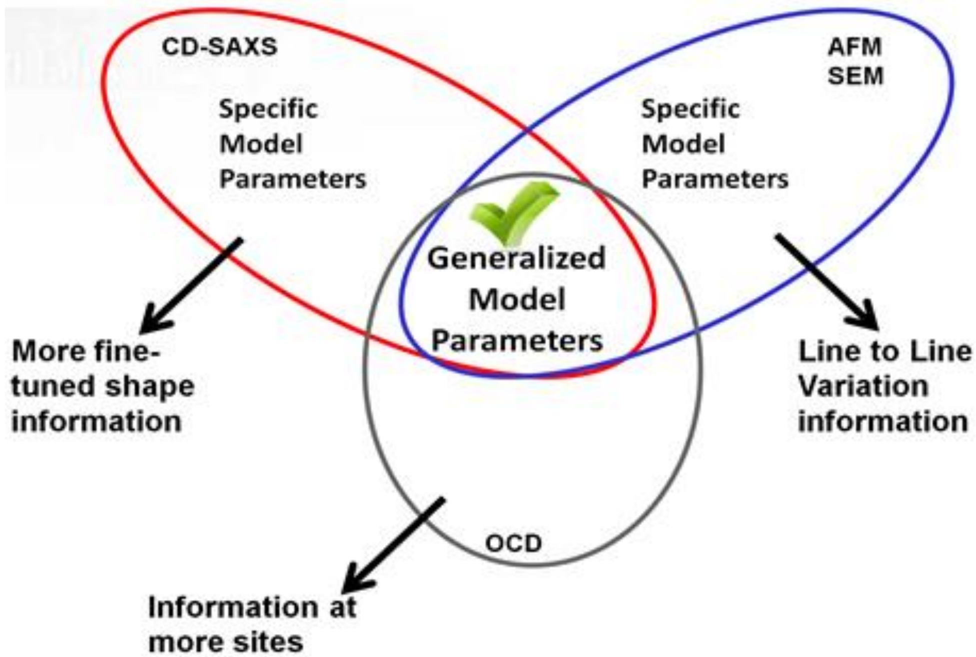

Figure 24: Conceptual diagram of hybrid metrology. Information from different instruments is used to develop a generalized model of the measurement. (*Image courtesy of Richard Silver NIST*).

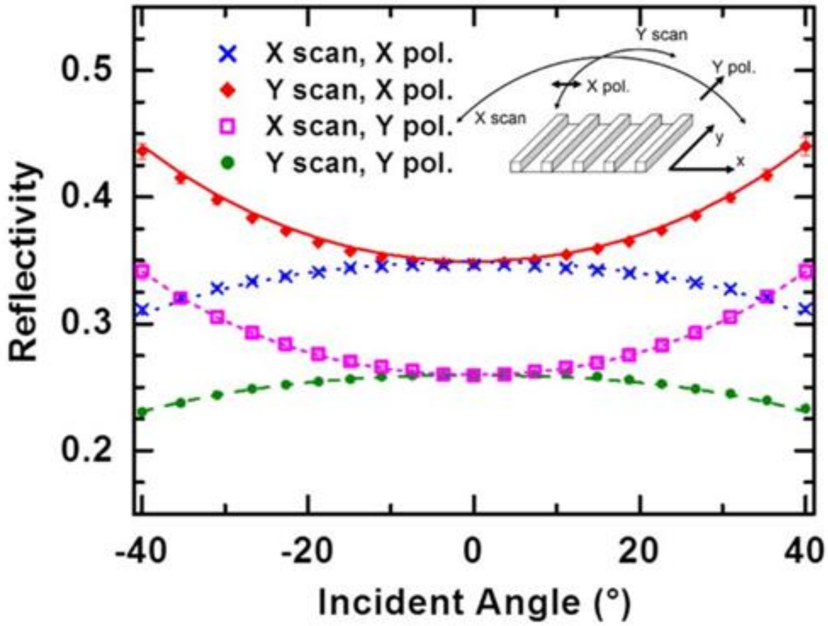

Figure 25: Experimental data (markers) and library data fits (curves) for the reflectivity from a patterned nitride line array on polysilicon. The curves in each plot correspond to the four combinations of scan direction and orthogonal linear polarizations shown in the top right corner of the plot. *(Image from Zhang et al. [66], used with permission*)

Table 3: Results from Parametric Fits to Data in Figure 23 Before and After Inclusion of Data from AFM

	OCD Only $\hat{a}_k(\sigma_{\hat{a}_k})$	AFM Only $a_k^*(\sigma_{a_k^*})$	Combined OCD and AFM With top, mid, height $\hat{a}_k(\sigma_{\hat{a}_k})$
Top (nm)	33.7 (10.8)	37.6 (0.9)	38.0 (0.9)
Middle (nm)	48.9 (6.0)	48.0 (1.9)	48.9 (1.8)
Bottom (nm)	68.9 (8.3)	*52.8 (3.3)*	66.6 (2.7)
Height (nm)	60.0 (2.2)	57.5 (0.7)$*$	58.6 (0.4)
n (% of nominal)	98.0 (1.0)		98.5 (0.5)

(from Zhang et al. [66], used with permission)

4. LIMITATIONS OF 3D-AFM AND POSSIBLE SOLUTIONS

Although 3D-AFMs are suitable for a wide variety of semiconductor measurements, there are major limitations that preclude wider adoption. The most important limitation is tip size. As the size of patterned lines continues to shrink, current 3D-AFM tips will not be able to profile dense lines and features. There are currently 10 nm diameter cylindrical CDAFM tips available[70], but further reduction in tip width will be required. A solution could be the use of CNT tips, but further research is needed on tip bending [71].

Another limitation is the relatively slow measurement time for AFMs in general. Although scan speed has improved over the years, 3D-AFMs are still much slower than scanning electron microscopes, where the move-acquire-measure time could be seconds. Even when such comparisons are unreasonable due to differences in the measurand, perception of low throughput could mean research funding being directed to tools that are perceived to be faster. Some industrial users have worked around throughput limitations by using the 3D-AFM only in high value measurements such as reference metrology. However, with the introduction of complex shaped features that require 3D characterization the need for faster scan speeds will be greater.

The need for tip shape removal and surface reconstruction will also grow as more 3D structures are introduced in the industry. Some work on improving tip shape characterization is ongoing, but the associated algorithms are not yet commercialized [40, 72]. There are tips available with very small edge heights to accurately capture surface deviations [70]. The existing techniques [13] do a great job of evaluating and reconstructing the tip and surface, but additional methods will be needed. Improvements in all aspects of tip size and shape characterization, tip manufacturing and surface reconstruction would need to continually improve in order to keep up with the measurement needs of complex 3D features.

One approach that could help is the increased use of modelling in addition to measurements to get needed results. To a large extent, this is already done for tip shape characterization. But as shown by Cordes et al. some combinations of scanning modes and tip types produce results that are more variable than others [73]. Additional models that include tip type, shape, feature shapes, tip-sample interaction, and scanner dynamics would be helpful in understanding measurement results. Given the level of uncertainties required for some measurands, an increased understanding of the behavior of the instrument in different measurement scenarios would be an important.

As mentioned above, there is no true 3D-AFM in the market today. Unfortunately, the technology is needed now than ever before. Although there is no inherent fundamental physics barrier to force sensing and feedback in three-axes, the implementation details are nontrivial. Things such as cross-talk among forces in different axes (especially for small features), scan algorithm implementation, and error separation techniques would need to be addressed. Also, alternatives to raster scanning may be needed for certain features. There is some work on cantilever response in 3D for topography measurements [74], but additional research by both commercial and non-commercial entities is needed.

5. CONCLUSION AND OUTLOOK

This chapter introduced the reader to different types of 3D AFM measurements for semiconductor metrology. We described different implementations of 3D-AFM, calibrations, and applications. The goal was to explore some of the key issues and give the reader a strong foundation for further study.

As feature sizes continue to shrink, and three dimensional and complex shape transistors are adopted by more integrated circuit manufacturers, the need for the types of measurements made by 3D-AFM will increase. The fundamentals of 3D-AFM technologies are well suited for these types of measurements, but would need continuous improvement and research in all aspects of the technology. Figure 26 shows a typical technology ramp curve for an established wafer generation. As shown in the figure, alpha tools should be in place at least 24 months before production. This refers to tools in general, not just those for metrology. For atomic force microscopes, a good portion of the work at this point involves developing suitable tips for feature sizes and materials involved, scanners, and scanning algorithms. With regards to materials, although AFM's topography contrast is relatively insensitive to material differences, it is not always negligible, especially with small tip sizes. At least some effort is made to ensure that appropriate coatings are used to prevent tip sticking. Note that the figure 26 covers Development and Production periods; there is an additional research period where the same metrology tools may be needed to adequately verify printability. The need to have tools available well before production underscores the need for more research in this area, for current and new technologies.

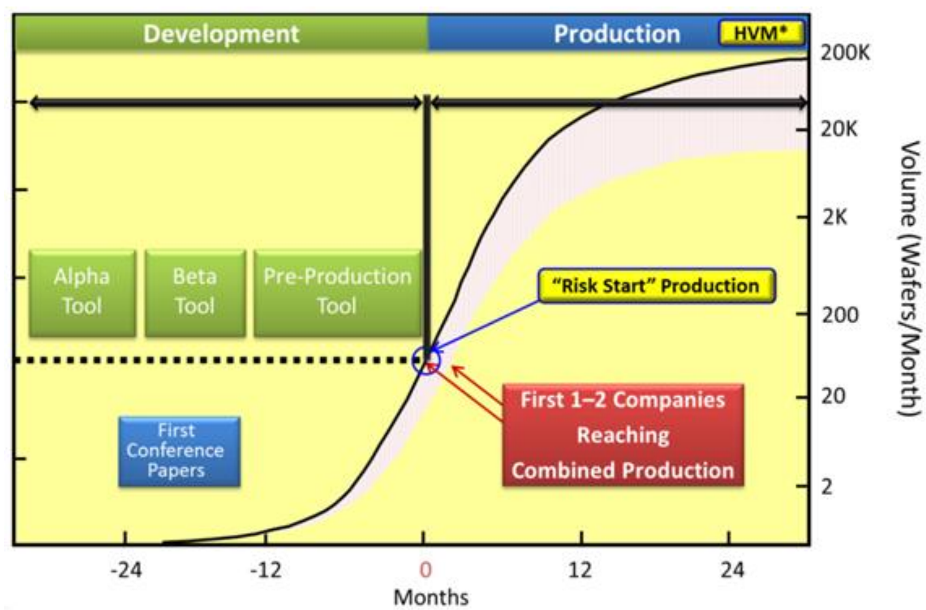

Figure 26: A typical technology production ramp curve for an established wafer generation. HVM stands for high volume manufacturing. (*ITRS Executive Summary 2011[19], used with permission*.)

In terms of current technology, due to the increasing complexity of semiconductor measurements, use of strategies such as hybrid or complementary techniques will increase, and may well be the dominant application of 3D-AFM. Research is already being done on how to leverage all aspects of the measurement process to solve critical dimension measurement needs [50], and this will only continue. As the use of finFETs increase, the CD-AFM is well suited for materials and electrical characterization on the sidewall. There is some interest by IC manufactures for this application, but no commercial instruments exist. This will likely change and will constitute a major improvement in the capabilities of the instrument. Developing new characterization techniques for tip width and shape characterization, surface reconstructions, and refinements of traceability evaluations techniques would need to proceed at a much faster pace than in the past. Although the primary application has been in semiconductor manufacturing, new uses in areas such as nanoparticles and nanoelectromechanical devices will increase.

6. ACKNOWLEDGEMENTS

We thank Yaw Obeng and Nicholas Dagalakis of NIST, and Vladimir Ukraintsev of Nanometrology, Inc. for reviewing the manuscript and providing valuable comments. We also thank the editors for inviting us to contribute a chapter, and authors that graciously allowed us to use their figures and materials. This work is funded by the Engineering Physics Division at NIST.

REFERENCES

1. Y. Martin and H. K. Wickramasinghe, *Magnetic imaging by ''force microscopy'' with 1000 Å resolution, Applied Physics Letters* **50** (20), 1455-1457 (1987). http://dx.doi.org/10.1063/1.97800

2. R. A. Oliver, *Advances in AFM for the electrical characterization of semiconductors, Reports on Progress in Physics* **71** (7), 076501 (2008). http://dx.doi.org/10.1088/0034-4885/71/7/076501

3. S. E. Park, et al., *Comparison of scanning capacitance microscopy and scanning Kelvin probe microscopy in determining two-dimensional doping profiles of Si homostructures, J. Vac. Sci. & Technol. B* **24** (1), 404 (2006). http://dx.doi.org/10.1116/1.2162569

4. D. Sarid, *Scanning force microscopy with applications to electric, magnetic and atomic forces* (Wiley, 1992).

5. G. Binnig, et al., *Atomic Force Microscope, Physical Review Letters* **56** (9), 930-933 (1986). http://dx.doi.org/10.1103/physrevlett.56.930

6. J. E. Griffith and D. A. Grigg, *Dimensional metrology with scanning probe microscopes, Journal of Applied Physics* **74** (9), R83-R109 (1993). http://dx.doi.org/10.1063/1.354175

7. D. Nyyssonen, *Two-dimensional atomic force microprobe trench metrology system, J. Vac. Sci. & Technol. B* **9** (6), 3612 (1991). http://dx.doi.org/10.1116/1.585855

8. G. L. Miller, et al., *A rocking beam electrostatic balance for the measurement of small forces, Review of Scientific Instruments* **62** (3), 705-709 (1991). http://dx.doi.org/10.1063/1.1142071

9. Y. Martin and H. K. Wickramasinghe, *Method for imaging sidewalls by atomic force microscopy, Applied Physics Letters* **64** (19), 2498-2500 (1994). http://dx.doi.org/10.1063/1.111578

10. N. G. Orji, et al., *Toward accurate feature shape metrology*, in *Proc. SPIE*, 6922, 692208 (SPIE, 2008). http://dx.doi.org/10.1117/12.774426

11. N. G. Orji, et al., *Line edge roughness metrology using atomic force microscopes, Measurement Science and Technology* **16** (11), 2147 (2005). https://doi.org/10.1088/0957-0233/16/11/004

12. D. Chen, et al., *Apparatus and method for determining side wall profiles using a scanning probe microscope having a probe dithered in lateral directions*, Patent No. US Patent 6,169,281 (2001).

13. G. Dahlen, et al., *Tip characterization and surface reconstruction of complex structures with critical dimension atomic force microscopy, J. Vac. Sci. & Technol. B* **23** (6), 2297 (2005). http://dx.doi.org/10.1116/1.2101601

14. N. G. Orji, et al., *Progress on implementation of a CD-AFM-based reference measurement system*, in *Proc. SPIE*, 6152, 61520O (SPIE, 2006). https://doi.org/10.1117/12.653287

15. T. Morimoto, et al., *Atomic Force Microscopy for High Aspect Ratio Structure Metrology, Japanese Journal of Applied Physics* **41** (Part 1, No. 6B), 4238-4241 (2002). http://dx.doi.org/10.1143/jjap.41.4238

16. M. Watanabe, *Atomic force microscope method for sidewall measurement through carbon nanotube probe deformation correction, J. Micro/Nanolith. MEMS MOEMS* **11** (1), 011009 (2012). http://dx.doi.org/10.1117/1.jmm.11.1.011009

17. S.-J. Cho, et al., *Three-dimensional imaging of undercut and sidewall structures by atomic force microscopy, Review of Scientific Instruments* **82** (2), 023707 (2011). http://dx.doi.org/10.1063/1.3553199

18. G. Dai, *New developments at Physikalisch Technische Bundesanstalt in three-dimensional atomic force microscopy with tapping and torsion atomic force microscopy mode and vector approach probing strategy, J. Micro/Nanolith. MEMS MOEMS* **11** (1), 011004 (2012). http://dx.doi.org/10.1117/1.jmm.11.1.011004

19. *International Technology Roadmap for Semiconductors, 2011 Edition*. San Jose: (Semiconductor Industry Association (SIA), 2011).

20. http://newsroom.intel.com/community/intel_newsroom/blog/2014/08/11/intel-discloses-newest-microarchitecture-and-14-nanometer-manufacturing-process-technical-details (*Last accessed*: 04/15/2015).

21. B. Bunday, et al., *Gaps Analysis for CD Metrology Beyond the 22 nm Node*, in *Proc. SPIE* 8681, 86813B (SPIE, 2013). http://dx.doi.org/10.1117/12.2012472

22. B. C. Park, et al., *Application of carbon nanotube probes in a critical dimension atomic force microscope*, in *Proc. SPIE*, 6518, 651819 (SPIE, 2007). https://doi.org/10.1117/12.712326

23. V. Vartanian, et al., *TSV reveal height and dimension metrology by the TSOM method*, in *Proc. SPIE*, 8681, 86812F (SPIE, 2013). https://doi.org/10.1117/12.2012609

24. F. Meli and R. Thalmann, *Long-range AFM profiler used for accurate pitch measurements, Measurement Science and Technology* **9** (7), 1087-1092 (1998). http://dx.doi.org/10.1088/0957-0233/9/7/014

25. R. G. Dixson, et al., *Dimensional metrology with the NIST calibrated atomic force microscope*, in *Proc. SPIE*, 3677, (SPIE, 1999). http://dx.doi.org/10.1117/12.350822

26. S. Gonda, et al., *Real-time, interferometrically measuring atomic force microscope for direct calibration of standards, Review of Scientific Instruments* **70** (8), 3362-3368 (1999). http://dx.doi.org/10.1063/1.1149920

27. G. B. Picotto and M. Pisani, *A sample scanning system with nanometric accuracy for quantitative SPM measurements, Ultramicroscopy* **86** (1-2), 247-254 (2001). http://dx.doi.org/10.1016/s0304-3991(00)00112-1

28. V. Korpelainen, *Measurement strategies and uncertainty estimations for pitch and step height calibrations by metrological atomic force*

microscope, J. Micro/Nanolith. MEMS MOEMS **11** (1), 011002 (2012). http://dx.doi.org/10.1117/1.jmm.11.1.011002

29. R. G. Dixson, et al., *Multilaboratory comparison of traceable atomic force microscope measurements of a 70-nm grating pitch standard, J. Micro/Nanolith. MEMS MOEMS* **10** (1), 013015 (2011). https://doi.org/10.1117/1.3549914

30. T. V. Vorburger, et al., *In the rough, Opt. Eng. Mag.*, 31–34 (2002). https://doi.org/10.1117/2.5200203.0008

31. N. G. Orji, et al., *Measurement traceability and quality assurance in a nanomanufacturing environment, J Micro-Nanolith Mem* **10** (1), 013006 (2011). https://dx.doi.org/10.1117/1.3549736

32. N. G. Orji, *Progress on implementation of a reference measurement system based on a critical-dimension atomic force microscope, J. Micro/Nanolith. MEMS MOEMS* **6** (2), 023002 (2007). http://dx.doi.org/10.1117/1.2728742

33. R. G. Dixson, et al., *Traceable calibration of critical-dimension atomic force microscope linewidth measurements with nanometer uncertainty, J. Vac. Sci. & Technol. B* **23** (6), 3028 (2005). http://dx.doi.org/10.1116/1.2130347

34. M. Tortonese, et al., *Sub-50-nm isolated line and trench width artifacts for CD metrology*, in *Proc. SPIE*, 5375, (SPIE, 2004). http://dx.doi.org/10.1117/12.536812

35. G. Dai, et al., *Reference nano-dimensional metrology by scanning transmission electron microscopy, Measurement Science and Technology* **24** (8), 085001 (2013). http://dx.doi.org/10.1088/0957-0233/24/8/085001

36. N. G. Orji, et al., *TEM calibration methods for critical dimension standards*, in *Proc. SPIE*, 6518, 651810 (SPIE, 2007). http://dx.doi.org/10.1117/12.713368

37. M. W. Cresswell, et al., *RM 8111: Development of a Prototype Linewidth Standard, Journal of Research of the National Institute of Standards and Technology* **111** (3), 187 (2006). http://dx.doi.org/10.6028/jres.111.016

38. C. McGray, et al., *Robust auto-alignment technique for orientation-dependent etching of nanostructures, J. Micro/Nanolith. MEMS MOEMS* **11** (2), 023005 (2012). https://doi.org/10.1117/1.JMM.11.2.023005

39. R. G. Dixson, et al., *Traceable calibration of a critical dimension atomic force microscope, J. Micro/Nanolith. MEMS MOEMS* **11** (1), 011006 (2012). https://doi.org/10.1117/1.JMM.11.1.011006

40. X. Qian and J. S. Villarrubia, *General three-dimensional image simulation and surface reconstruction in scanning probe microscopy using a dexel representation, Ultramicroscopy* **108** (1), 29-42 (2007). http://dx.doi.org/10.1016/j.ultramic.2007.02.031

41. N. G. Orji and R. G. Dixson, *Higher order tip effects in traceable CD-AFM-based linewidth measurements, Measurement Science and Technology* **18** (2), 448-455 (2007). http://dx.doi.org/10.1088/0957-0233/18/2/s17

42. R. Dixson and N. G. Orji, *Comparison and uncertainties of standards for critical dimension atomic force microscope tip width calibration*, in *Proc. SPIE*, 6518, 651816 (SPIE, 2007). https://doi.org/10.1117/12.714032

43. R. Dixson, et al., *Interactions of higher order tip effects in critical dimension-AFM linewidth metrology, J. Vac. Sci. & Technol. B* **33** (3), 031806 (2015). https://doi.org/10.1116/1.4919090

44. G. W. Banke and C. N. Archie, *Characteristics of accuracy for CD metrology*, in *Proc. SPIE*, 3677, (SPIE, 1999). http://dx.doi.org/10.1117/12.350818

45. L. J. Lauchlan, et al., *Metrology Methods in Photolithography*, in *Handbook of Microlithography, Micromachining, and Microfabrication. Volume 1: Microlithography* (SPIE, 1997). http://dx.doi.org/10.1117/3.2265070.ch6

46. H. Marchman, *Scanning electron microscope matching and calibration for critical dimensional metrology*, *J. Vac. Sci. & Technol. B* **15** (6), 2155 (1997). http://dx.doi.org/10.1116/1.589344

47. V. Ukraintsev and B. Banke, *Review of reference metrology for nanotechnology: significance, challenges, and solutions*, *J. Micro/Nanolith. MEMS MOEMS* **11** (1), 011010 (2012). http://dx.doi.org/10.1117/1.jmm.11.1.011010

48. J. Foucher, et al., *Hybrid metrology for critical dimension based on scanning methods for IC manufacturing*, in *Proc. SPIE*, 8378, 83780F (SPIE, 2012). http://dx.doi.org/10.1117/12.919650

49. A. Vaid, et al., *Hybrid metrology: from the lab into the fab*, *J. Micro/Nanolith. MEMS MOEMS* **13** (4), 041410 (2014). http://dx.doi.org/10.1117/1.jmm.13.4.041410

50. J. Mandel, *Fitting Straight Lines When Both Variables are Subject to Error*, *Journal of Quality Technology* **16** (1), 1-14 (1984). http://dx.doi.org/10.1080/00224065.1984.11978881

51. M. Sendelbach and C. N. Archie, *Scatterometry measurement precision and accuracy below 70 nm*, in *Proc. SPIE* 5038, (SPIE, 2003). http://dx.doi.org/10.1117/12.488117

52. B. Bunday, et al., *Impact of sampling on uncertainty: Semiconductor dimensional metrology applications*, in *Proc. SPIE*, 6922, 69220X (SPIE, 2008). https://doi.org/10.1117/12.772993

53. N. Rana, et al., *The measurement uncertainty challenge of advanced patterning development*, in *Proc. SPIE*, 7272, 727203 (SPIE, 2009). http://dx.doi.org/10.1117/12.814170

54. B. N. Taylor, *Guidelines for evaluating and expressing the uncertainty of NIST measurement results*. (NIST, 1994).

55. B. Bunday, et al., *The coming of age of tilt CD-SEM*, in *Proc. SPIE* 6518, 65181S (SPIE, 2007). https://doi.org/10.1117/12.714214

56. B. Bunday, et al., *Characterization of CD-SEM metrology for iArF photoresist materials*, in *Proc. SPIE*, 6922, 69221A (SPIE, 2008).

57. J. Clarke, et al., *Photoresist cross-sectioning with negligible damage using a dual-beam FIB-SEM: A high throughput method for profile imaging, J. Vac. Sci. & Technol. B* **25** (6), 2526-2530 (2007). https://doi.org/10.1116/1.2804516

58. N. G. Orji, et al., *Measurement traceability and quality assurance in a nanomanufacturing environment*, in *Proc. SPIE*, 7405, 740505 (SPIE, 2009). https://doi.org/10.1117/12.826606

59. D. Hibino, et al., *High-accuracy optical proximity correction modeling using advanced critical dimension scanning electron microscope-based contours in next-generation lithography, J Micro-Nanolith Mem* **10** (1) (2011). https://www.doi.org/10.1117/1.3530082

60. J. S. Villarrubia, et al., *Proximity-associated errors in contour metrology*, in *Proc. SPIE*, 7638, 76380S (SPIE, 2010). http://dx.doi.org/10.1117/12.848406

61. Y.-A. Shim, et al., *Methodology to set-up accurate OPC model using optical CD metrology and atomic force microscopy*, in *Proc. SPIE*, 6518, 65180C (SPIE, 2007). http://dx.doi.org/10.1117/12.711936

62. V. A. Ukraintsev, *Role of CDAFM in achieving accurate OPC modeling*, in *Proc. SPIE*, 7272, 727205 (SPIE, 2009). http://dx.doi.org/10.1117/12.815240

63. N. G. Orji, et al., *Strategies for nanoscale contour metrology using critical dimension atomic force microscopy*, in *Proc. SPIE*, 8105, 810505 (SPIE, 2011). https://doi.org/10.1117/12.894416

64. N. G. Orji, et al., *Contour metrology using critical dimension atomic force microscopy*, in *Proc. SPIE* 8324, 83240U (SPIE, 2012). https://doi.org/10.1117/12.918056

65. T. H. McWaid, et al., *Methods divergence between measurements of micrometer and sub-micrometer surface features*, *Nanotechnology* **5** (1), 33-43 (1994). http://dx.doi.org/10.1088/0957-4484/5/1/004

66. N. F. Zhang, et al., *Improving optical measurement uncertainty with combined multitool metrology using a Bayesian approach*, *Applied Optics* **51** (25), 6196 (2012). http://dx.doi.org/10.1364/ao.51.006196

67. N. Rana, et al., *Leveraging advanced data analytics, machine learning, and metrology models to enable critical dimension metrology solutions for advanced integrated circuit nodes, J. Micro/Nanolith. MEMS MOEMS* **13** (4), 041415 (2014). http://dx.doi.org/10.1117/1.jmm.13.4.041415

68. A. Vaid, *Holistic metrology approach: hybrid metrology utilizing scatterometry, critical dimension-atomic force microscope and critical dimension-scanning electron microscope, J. Micro/Nanolith. MEMS MOEMS* **10** (4), 043016 (2011). http://dx.doi.org/10.1117/1.3655726

69. A. Vaid and E. Solecky, *Special Section Guest Editorial: Holistic/Hybrid Metrology, J. Micro/Nanolith. MEMS MOEMS* **13** (4), 041401 (2014).

70. J. Foucher, et al., *Manufacturing and advanced characterization of sub-25nm diameter CD-AFM probes with sub-10nm tip edges radius*, in *Proc. SPIE*, 8681, 86811I (SPIE, 2013). http://dx.doi.org/10.1117/12.2011451

71. V. A. Ukraintsev, et al., *Distributed force probe bending model of critical dimension atomic force microscopy bias, J. Micro/Nanolith. MEMS MOEMS* **12** (2), 023009 (2013). http://dx.doi.org/10.1117/1.jmm.12.2.023009

72. H. Takenaka, et al., *Development of Si/SiO₂ Multilayer Type AFM Tip Characterizers, Journal of Surface Analysis* **17** (3), 264-268 (2011). http://dx.doi.org/10.1384/jsa.17.264

73. A. Cordes, *Sidewall slope sensitivity of critical dimension atomic force microscopy, J. Micro/Nanolith. MEMS MOEMS* **11** (1), 011011 (2012). http://dx.doi.org/10.1117/1.jmm.11.1.011011

74. W. Häßler-Grohne, et al., *Investigation of the cantilever response of non-contact atomic force microscopy for topography measurements in all three dimensions, Measurement Science and Technology* **22** (9), 094006 (2011). http://dx.doi.org/10.1088/0957-0233/22/9/094006